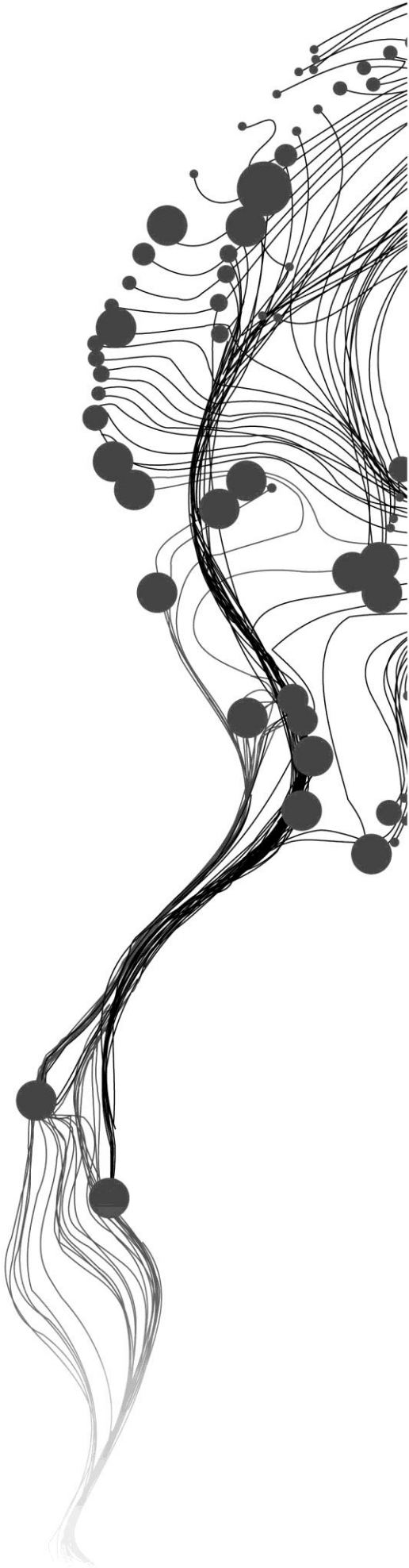


# **SYNTHETIC APERTURE RADAR FOR VEGETATION AND SOIL MOISTURE MONITORING IN MASAI MARA**

NYANG'ACHA DAVID ONGO  
March, 2015

SUPERVISORS:  
Dr. Ir. Rogier van der Velde  
Dr. Zoltán Vekerdy



# **SYNTHETIC APERTURE RADAR FOR VEGETATION AND SOIL MOISTURE MONITORING IN MASAI MARA**

NYANG'ACHA DAVID ONGO

Enschede, The Netherlands, March, 2015

Thesis submitted to the Faculty of Geo-Information Science and Earth Observation of the University of Twente in partial fulfilment of the requirements for the degree of Master of Science in Geo-information Science and Earth Observation.

Specialization: Water Resources and Environmental Management

THESIS ASSESSMENT BOARD:

Chairman: Prof. Dr. Ing. W. Verhoef

External Examiner: Dr. H van der Kwast (UNESCO-IHE Delft)

Dr. Ir. R. van der Velde

Dr. Z. Vekerdy

#### DISCLAIMER

This document describes work undertaken as part of a programme of study at the Faculty of Geo-Information Science and Earth Observation of the University of Twente. All views and opinions expressed therein remain the sole responsibility of the author, and do not necessarily represent those of the Faculty.

## ABSTRACT

The Mara River Basin (MRB) is an important catchment both in Kenya and Tanzania. The Mau forest and Masai Mara wildlife reserve are important ecosystems located within MRB. This study is part of the larger Mau-Mara-Serengeti (MaMaSe) sustainable water initiative aimed at improving water safety and security in MRB. The main objective of this research is to evaluate the effects of vegetation on SAR backscatter using dual polarized RADARSAT-2 (RS2) Synthetic Aperture Radar (SAR) C-band over Masai Mara, between May 2011 and August 2012. This is to investigate the feasibility of using Sentinel-1 (S1) SAR C-band for vegetation and soil moisture monitoring over the MRB.

As part of long term soil moisture monitoring, a description of the installation of near real time soil moisture monitoring stations, Kenya Mara Station (KMST) is given. KMST01 was destroyed and the instruments recovered from the field site.

Dual polarized RS2 VV+VH and MODIS NDVI were used to study temporal and spatial variability of RS2 backscatter. There was a positive correlation of RS2 and MODIS NDVI in cropland and savannah. Cropland showed the highest coefficient of determination ( $R^2$ ) of 0.58 with VH polarization for the whole study period. Permanent vegetation showed insignificant relationship. Depolarization ratio (VV-VH) of RS2 was derived and it showed a positive relationship with MODIS NDVI, this agreement showed that the ratio can be used in vegetation monitoring. The standardized backscatter anomalies (anomaly maps) were derived both for RS2 and un-calibrated S1 data. The anomaly maps showed the variation of soil moisture. In-situ measurements derived from (KMST) was compared to S1 anomaly maps, the comparison showed agreement between the datasets. A visual comparison of RS2 and S1 anomaly maps showed similar pattern, thus showing potential of using S1 to carry out a similar study.

**Keywords:** Sentinel-1, SAR, Depolarization ratio, standardized anomaly

To MY PARENTS AND FAMILY  
WE ALL DID IT  
THANKS BE TO GOD

## ACKNOWLEDGEMENTS

I am deeply and greatly indebted to the Dutch government and Netherlands Fellowship Program (NFP) committee for offering me the scholarship. The scholarship enabled me complete my studies without much financial struggle. I cannot go without thanking MaMase project for funding the fieldwork, including purchase of field equipment in order to complete my research.

To my supervisors, I have no words to express my gratitude to you, and I can't thank you enough. I would like to thank my first supervisor Dr. Ir. Rogier van der Velde for his mentorship on SAR processing and interpretation, unrelenting support and constantly furnishing me with new ideas on how to shape my research, for helping me with scripts when some of the software took too long to process the data and for compiling our fieldwork report for these and many more, thank you so much. My sincere heartfelt gratitude goes to Dr. Zoltan vekerdy for his critical review of this work, his advice, his concern and care too set up a meeting with ESA people in order to get the right data, at some point we had to Skype in order to help me out, thank you sir.

Special thanks goes to the my friends and classmate and particularly Henry gathecha and PhD candidate Omar eweys for their fieldwork support and installation of the KMST in Mara reserve and surrounding conservancies, thanks to Omar for his support and guide in soil analysis. Thank you for your support, wish you all the best in all your endeavors.

Immense gratitude goes to the Daniel kuyo, Dennis, Muntet of Embiti primary school, staff members at Nkoilale primary school for allowing us to setup our soil moisture stations, without forgetting James maingi for his skilful driving over the rough terrain and good knowledge of the Masai Mara region.

Special thanks go to Nourhan morsy for her constant motivation when things got tougher and materials to help me out, I owe you one. Without forgetting Dennis onyango, Jared buoga, Vella kwamboka, Benson maina for sharing their knowledge about Masai Mara and for being part of MaMaSe project, thank you guys.

To my family especially my dear parents, it's your motivation that has always pushed me forward, thank you for being great parents.

I am grateful to all those who in on one way or another made it possible for the smooth running of my studies at ITC.

Above all I thank God for His grace throughout the study period.

# TABLE OF CONTENTS

---

1.	Introduction .....	1
1.1.	Background.....	1
1.2.	Societal context of the study .....	2
1.3.	Problem statement .....	2
1.4.	Research objectives .....	3
1.5.	Specific objectives .....	3
1.6.	Research questions .....	3
1.7.	Research method .....	3
1.8.	Thesis structure and outline .....	4
2.	Soil moisture retrieval methods.....	5
2.1.	In-situ soil moisture .....	5
2.2.	Microwave remote sensing of soil moisture .....	5
2.3.	Soil dielectric properties .....	6
2.4.	Impact of vegetation on radar backscatter.....	6
3.	Description of the study area .....	8
3.1.	River Basin.....	8
3.2.	Hydrometeorology .....	9
3.3.	Topography and soil .....	9
3.4.	Socio-economic activities.....	10
4.	In Situ Data .....	12
4.1.	Kenya Mara Soil Moisture Station.....	12
4.2.	The network .....	14
4.3.	Calibration .....	15
4.4.	Organic matter determination.....	16
4.5.	Particle size analysis .....	17
5.	Satellite Data.....	19
5.1.	Tropical Rainfall Measuring Mission (TRMM) .....	19
5.2.	Digital Elevation Model .....	19
5.3.	MODIS NDVI .....	20
5.4.	RADARSAT-2.....	21
5.5.	Sentinel-1 .....	22
6.	Satellite Data Processing .....	25
6.1.	SAR Data .....	25
6.2.	MODIS NDVI .....	26
6.3.	TRMM 3B42v7 rainfall.....	26
7.	Results and Discussion .....	27
7.1.	Kenya Mara Soil Moisture Station.....	27
7.2.	Temporal backscatter analysis of RADARSAT 2, Rainfall and MODIS NDVI .....	29
7.3.	RADARSAT-2 depolarization ratio .....	34
7.4.	Spatial backscatter variability and standardized anomaly .....	37
7.5.	Sentinel-1 Analysis.....	41
7.6.	Comparison between Sentinel-1 and RADARSAT-2.....	43
8.	Conclusion and Recommendations .....	44
8.1.	Conclusion.....	44
8.2.	Recommendations.....	44

## LIST OF FIGURES

---

Figure 1: Research workflow .....	4
Figure 2: Scattering of an incident radar signal by a rough and vegetated surface. Adapted from (Kornelsen & Coulibaly, 2013).....	7
Figure 3: Mara River Basin. (Data source :Dessu et al., 2014).....	8
Figure 4: Topography of Mara River Basin (Source: ITC database).....	9
Figure 5: Soil texture within the Mara River Basin (Data source: ILRI).....	10
Figure 6: Land cover classes within the Mara basin ecosystem (Data source: ILRI).....	11
Figure 7: Topographic map of the Masai Mara reserve (Purple boundaries) and surrounding conservancies on top of which polygons are shown of areas that have fairly uniform statistics properties deduced from a 14 year long time series of MODIS NDVI (Courtesy Kees de bie) .....	12
Figure 8: False color composite (R: band4, G: band3, B: band2) of a Landsat 5TM acquisition taken on 12 July 2011 indicating the location of the soil moisture monitoring stations. ....	14
Figure 9: General landscape locations of KMST .....	15
Figure 10: Probe soil moisture plotted against gravimetric soil moisture content, (A) all stations, (B) KMST01, 04, 05 and 06, (C) KMST02 and 03 (Rogier van der Velde et al., 2014). ....	16
Figure 11: Particle size distribution of the location each KMST.....	18
Figure 12: Measurement instruments onboard TRMM satellite (NASA, 2014b).....	19
Figure 13: Observation geometries and coverage modes of RADARSAT-2. Image retrieved from ( <a href="https://directory.eoportal.org">https://directory.eoportal.org</a> ).....	21
Figure 14: Sentinel-1 image acquisition modes (Source: ESA, 2014) .....	22
Figure 15: Sentinel-1 product naming convention (Source: ESA, 2014). ....	24
Figure 16: Un-calibrated sentinel-1 SAR intensity image.....	24
Figure 17: Effect of speckle filtering as a function of filter sizes on interpretability of a SAR image (Sentinel-1 image of 4 October 2014).....	25
Figure 18: Examples of antenna setups improvised to increase the reception with the telecommunication network for the remote exchange of data. ....	27
Figure 19: Measured temperature and soil moisture of the KMST in Masai Mara. ....	28
Figure 20: Inundation land surface conditions destroyed the electronics of the data logger at KMST01 after which communication stopped on September 25 <sup>th</sup> 2014. ....	29
Figure 21: Daily rainfall distribution and seasonal transition of Masai Mara from May 2011 – August 2012 .....	29
Figure 22: Temporal variation of MODIS NDVI and RS2 Backscatter polarization on the whole study area.....	30
Figure 23: Comparison between RS2 and MODIS NDVI data over cropland, permanent vegetation and savanna land.....	31
Figure 24: Seasonal variation of MODIS NDVI and RS2 backscattering coefficient over cropland .....	31
Figure 25: Seasonal variation of MODIS NDVI and RS2 backscattering coefficient over savanna grassland.....	32
Figure 26: Seasonal variation of MODIS NDVI and RS2 backscattering coefficient over permanent vegetation.....	33
Figure 27: Temporal correlation of MODIS NDVI and RS2 Backscattering coefficient.....	34
Figure 28: Generic characteristic of depolarization ratio.....	35
Figure 29: Depolarization ratio of RS2 VH (dB) - VV (dB) showing plots for Cropland, Savanna land and Permanent vegetation. ....	35

Figure 30: Variation of the ratio VH (dB) to VV (dB) plotted against MODIS NDVI over selected land cover a) cropland b) Savanna grassland c) Permanent vegetation.....	36
Figure 31: RGB composite of 2 RS2 SAR for dry (19 Jan 2012) and wet (18 May 2012) season. The composites were made of R (VV), G (VH), and B (VV).....	37
Figure 32: Mean and standard deviation of RADARSAT 2 VV polarization. ....	38
Figure 33: Spatial backscatter variability as a function of mean and standard deviation. ....	40
Figure 34: Standardized backscatter anomaly of (Un-calibrated) Sentinel-1.....	41
Figure 35: K MST measurements of soil moisture and soil temperature.....	42
Figure 36: Comparison between Sentinel-1 and RADARSAT 2.....	43

## LIST OF TABLES

---

Table 1: Description of the polygons shown in figure 10 representing the largest areas with each uniform long-term NDVI statistics (i.e. median, standard deviation) deduced from a 14 years MODIS NDVI data set. The colors correspond to argumentation for (not) sampling. ....	13
Table 2: List of monitoring stations installed in the Masai Mara Reserve and surrounding conservancies whereby the ID number corresponds to the polygons in Fig. 7. ....	14
Table 3: Calibration parameters for the decagon 5TM probe installed in the Masai Mara reserve and conservancy with associated error statistics. ....	16
Table 4: Soil texture (Clay, Silt, and Sand) for the five Mara stations installed in 2014. ....	18
Table 5: Summary of SRTM DEM Properties. ....	20
Table 6: MODIS NDVI image dates used for the study. ....	21
Table 7: Summary of RADARSAT-2 properties. ....	22
Table 8: Sentinel-1 main acquisition modes, courtesy (Torres et al., 2012). ....	23
Table 9: Sentinel-1 images available. ....	23
Table 10: Variation of Coefficient of determination ( $R^2$ ) over different vegetation types and seasons. ....	32
Table 11: Variation of Coefficient of determination ( $R^2$ ) over different vegetation types and seasons as a function of depolarization ratio. ....	36

## LIST OF ACRONYMS

---

AMSR-E	The Advanced Microwave Scanning Radiometer - Earth Observing satellite
ASCAT	Advanced Scatterometer
ASCII	American Standard Code for Information Interchange
DEM	Digital Elevation Model
ESA	European Space Agency
GMES	Global Monitoring of Environment for Security
GPS	Global Positioning System
IEM	Integral equation method
ILRI	International Livestock Research Institute
ITC	International Institute for Geo Information science and Earth observation
KMST	Kenya Mara Station (Soil Moisture)
KWS	Kenya Wildlife Services
MaMaSe	Mau-Mara-Serengeti ecosystem
MODIS	Moderate Resolution Imaging Spectroradiometer
MRB	Mara River Basin
NAMI	National Imagery and mapping Agency
NASA	National Aeronautic and Space Administration
NDVI	Normalized Difference Vegetation Index
NETCDF	Network Common Data Format
RS2	RADARSAT 2
S1	SENTINEL 1
S1TBX	Sentinel-1 toolbox
SAR	Synthetic Aperture Radar
SEBS	Surface Energy Balance System
SMAP	Soil Moisture Active Passive
SMOS	Soil Moisture Soil Salinity
SRTM	Shuttle Radar Topographic Mission
TIFF	Tagged Image File Format
TRMM	tropical Rainfall measuring mission
USDA	United States Department of Agriculture
VH	Vertical polarization on transmit, Horizontal polarization on receive
VSM	Volumetric Soil Moisture
VV	Vertical polarization on transmit, Vertical polarization on receive

# 1. INTRODUCTION

## 1.1. Background

'Water is life', this is a common saying used to depict the importance of water (in all its state) in supporting various forms of life in nature. In relation to plant life, it is well expressed when soil moisture diminishes and drying soils reach wilting point so plants cannot take up water anymore. More details are given in Tolk (2003). Soil moisture can be defined as the water above the water table (Brutsaert,2005). It is an important hydroclimatic variable that influences the hydrological cycle; other variables include precipitation, evapotranspiration, and vegetation. Hydrologic cycle involves mass and energy interchange between the Earth's surface and the atmosphere.

Understanding soil moisture is important, it partially controls runoff, which can lead to flooding and also it influences mass and energy fluxes between the land surface and atmosphere by evaporation (Sandells, Davenport, & Gurney, 2008). According to Seneviratne et al., 2010, soil moisture has an impact on the exchange of trace gases on land, including carbon dioxide. Various studies have observed the interactions of soil moisture, land surface and climate, these interactions influences the atmospheric boundary layer hence weather and global climate patterns (Patel, Anapashsha, Kumar, Sah, & Dadhwal, 2009). These climate patterns in turn influences human socio- economic activities (Seneviratne et al., 2010). Acquiring knowledge about soil moisture distribution is important in understanding vertical movement of water i.e. infiltration, percolation and evaporation, which, eventually determine distribution and growth of both flora and fauna. Water resources managers, ecologist, rangeland officers and farm managers will benefit from this kind of knowledge, as it will equip them with best ways to plan for available water resources, thus providing continuous food and clean water supply within their area of jurisdiction.

Soil moisture content varies over space and time especially at the soil surface. Spatial-temporal variability of soil moisture content is influenced by hydroclimatic variables in addition to topography, soil texture and land use. Petropoulos (2014) gives detailed description of factors influencing spatial-temporal variability of soil moisture. These variables make it difficult to accurately quantify soil moisture content over space and time (Van der Velde et al., 2012). The nature and importance of soil moisture has led to a variety of methods put in place for its quantification, i.e. in-situ and remote sensing methods. In-situ methods (field measurements) are widely used as a source of soil moisture point data. These methods are accurate. However, they have a limitation to spatial coverage in addition, to being expensive and time consuming. Remote sensing involves measuring of a phenomenon or object without being in direct contact with it. It can be subdivided into optical and microwave remote sensing (passive and active) (Lillesand, Kiefer, & Chipman, 2008). Remote sensing is playing a critical role in solving in-situ data problems like spatial and temporal coverage.

Continuous advances in remote sensing field have made it possible to retrieve soil moisture under a variety of field conditions (Engman & Chauhan, 1995; Bindlish & Barros, 2000). A number of techniques using different data types have been applied in measuring of soil moisture content within the electromagnetic spectrum e.g. optical and microwave part (Njoku & Kong, 1977; Rahimzadeh-Bajgiran et al., 2013; Su, 2009).

Optical remote sensing of soil moisture utilizes wavelengths ranging from 0.4 to 2.5 $\mu$ m, it measures reflected radiation of the sun from earth's surface (Petropoulos, 2014). This technique is based on several methods that seek to retrieve latent heat and sensible heat fluxes between the Earth's surface and the

atmosphere. These methods use minimal information in solving the surface energy balance. The thermal infrared technique utilizes wavelengths between 3.5 and 14 $\mu\text{m}$ , it is based upon thermal inertia to describe the impedance of soil to temperature. Su, 2002 gives an elaborate and insightful detail on the surface energy balance system (SEBS). Detailed description of the microwave portion is given in Chapter 2.

## **1.2. Societal context of the study**

The Mara River basin is a trans-boundary basin shared among Kenya and Tanzania. The basin harbours Mau forest which is an important water tower for Kenya and the Lake Victoria region. This region is dependent on water for socio-economic growth and environmental sustainability. Agricultural activities like crop farming and cattle rearing all depend upon availability of water. Wildlife migration within Masai Mara and Serengeti has been associated with water and pasture availability (UNESCO.IHE, 2014; Mati et al., 2008). Continuous degradation of environment through deforestation and encroachment of the Mau forest, poor agricultural activities and changing land practice on the upper part of the basin has led to rapid overland flow and soil erosion. Sedimentation of river Amala and Nyangores has been associated to soil erosion, while pollution is as a result of poor agricultural practices (UNESCO.IHE, 2014). The continuous river pollution of Amala and Nyangores has led to degradation of water quality. As large tracts of land are being converted to farmlands, there is need to protect the crops from animal destruction through fencing, this in turn has led to blockage of wildlife migration pathways and dispersal routes hence denying wildlife access to water. If the environmental degradation trend continues then agricultural activities, tourism and livelihoods will take a dive. Food insecurity, diseases and forced migration is likely to occur in the long run (Mati et al., 2008).

It is therefore important to control these causes to avoid further degradation through, careful strategic planning, continuous monitoring and realistic regulations of the various water authorities, optimal water usage for maximum production and water quality protection (UNESCO.IHE, 2014). Various hydrological tools exist for water resources management like hydrological models which require feeding of soil moisture. However, most of these hydrological models are still using in-situ measurements which are expensive, time consuming and has small spatial coverage therefore the need for soil moisture monitoring through remote sensing.

## **1.3. Problem statement**

Microwave remote sensing is sensitive to soil moisture, however, it is highly affected by vegetation, surface roughness and has low temporal resolution in comparison to optical remote sensing (Fung & Eom, 1985; Gherboudj et al., 2011). In spite of these limitations, passive microwave based coarse resolution (20-50 km) soil moisture products are available e.g. AMSR-E C-band (56 km), ASCAT (25km), SMOS (43 km) and SMAP was recently launched in January 2015. At finer scale, the potential of microwave remote sensing to soil moisture retrieval is limited to the type of sensor and continuity of the data provision (van der Velde et al., 2012). Most of the operational sensors like X-band, L-band and C-band SAR systems have low temporal resolution, while some are commercially operated thus the images are expensive e.g. RADARSAT 1 and 2. Some are free but are no longer in operation e.g. ENVISAT ASAR and ERS.

The European Earth observation programme, Copernicus, previously GMES (Global Monitoring for Environment and Security) is a system for monitoring the Earth. It is made up of a set of systems that obtain data from earth observation satellites (Sentinel-1, 2, 3) and in-situ sensors. Copernicus services are hinged on six thematic areas i.e. land, marine and atmospheric monitoring, climate change, emergency management and security (FDC, 1989). The themes are tailored to suit policy makers and public

authorities, who need the information in developing environmental legislation and policies or in critical decision making like natural disaster or humanitarian crisis (FDC, 1989).

The recent launch of Sentinel-1 Synthetic Aperture Radar (SAR) C-band is regarded as advancement to SAR data availability. Studies have shown (Torres et al., 2012; Gherboudj et al., 2011; Van der Velde et al., 2012; Paloscia et al., 2013) field code has changed and attention is shifting to multi-configuration radar, with capabilities of multiple polarizations and multiple incidence angles. Operational modes of Sentinel-1 include, strip mode, interferometric mode, extra wide swath and wave mode. These modes offer products in single polarization horizontal (HH) or vertical (VV) and dual polarization (HH+VV or VV+VH), improved spatial resolution (10m), in addition to improved temporal resolution. Using these images with the right algorithm offers effective soil moisture retrieval (Gherboudj et al., 2011).

In this study, temporal and spatial of variation SAR data (Sentinel-1 and RADARSAT-2) was evaluated in relation to vegetation biomass in this case Normalized Difference Vegetation Index (NDVI). A ratio (depolarization ratio) obtained from the RADARSAR-2 dual polarization was also compared to vegetation biomass. The standardized anomaly of SAR data was used to study soil moisture variation. The study also describes the installation of near real time soil moisture monitoring network i.e. Kenya Mara Station (KMST).

#### 1.4. Research objectives

The main objective of this study is to evaluate the effects of vegetation on SAR backscatter using dual polarized RADARSAT-2 SAR C-band towards processing of sentinel-1 for soil moisture retrieval.

#### 1.5. Specific objectives

- To study the effects of vegetation on RADARSAT-2 SAR backscatter.
- To evaluate the dual polarization capabilities in vegetation monitoring.
- To evaluate satellite retrieved soil moisture to the in-situ soil moisture.

#### 1.6. Research questions

- What are the effects of natural (different rangelands) vegetation on the observed backscatter?
- How does the vegetation affect the Sentinel-1 and RADARSAT-2 observed backscatter and how can dual-polarized data be used to correct for it?
- How can depolarization ratio be used in vegetation monitoring?
- How does in situ soil measurements relate with SAR derived soil moisture?

#### 1.7. Research method

The procedure involves processing of satellite data in order to obtain pixel information. It includes pre-processing of SAR data in order to obtain backscatter values and processing of MODIS NDVI in order to obtain biomass values. The obtained values are coupled with TRMM rainfall estimates to carry out spatial and temporal backscatter analysis. Coefficient of determination ( $R^2$ ) was obtained for the full (year) season and for each season (wet or dry). A stack of SAR images were made separately (Sentinel-1, RADARSAT), this enabled calculation of mean and standard deviation of VH and VV. In addition, composite of

individual RS2 images was made in order to study spatial backscatter variation. Using the mean and the standard deviation, soil moisture anomaly was obtained for each image. Depolarization ratio was obtained by subtracting VV from VH (for only RS2). The ratio was also compared to MODIS NDVI values and  $R^2$  obtained for each season. A visual comparison of un-calibrated S1 standardized anomaly maps and in-situ soil measurements were done, and finally a visual comparison of S1 and RS2 was made. Figure 1 describes the procedure adopted in this study.

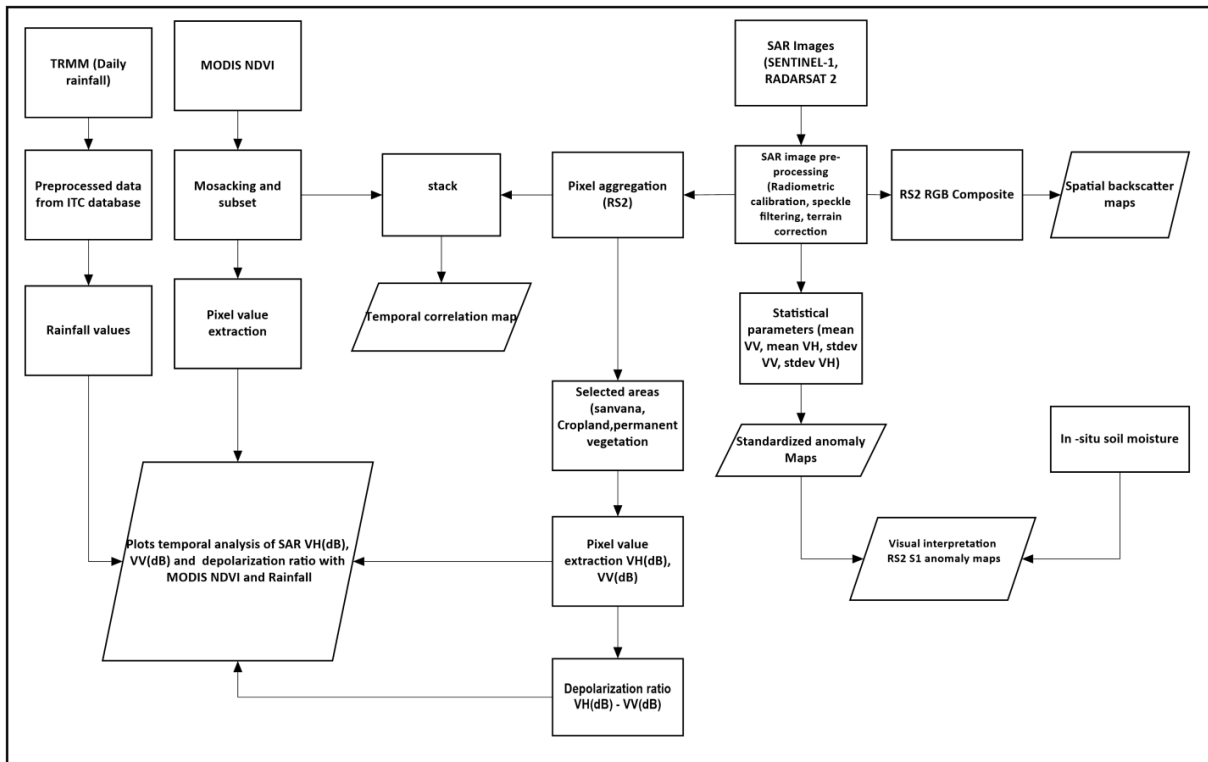


Figure 1: Research workflow

## 1.8. Thesis structure and outline

Chapter 1 (the present one) gives an introduction to the study, background, problem statement, societal context of the study, research objectives, research questions and the outline of the study. Chapter 2 reviews on previous studies in soil moisture, vegetation effect on backscatter as well as some methods that have been used in soil moisture retrieval. Chapter 3 gives an insight on the study area. Chapter 4 describes in-situ data sets used in this study. Chapter 5 gives detail in satellite data used. Chapter 6 explains the processing of satellite data adopted in the study to meet the set objectives. Results and discussions are outlined in chapter 7. Chapter 8 outlines conclusion and recommendations.

## 2. SOIL MOISTURE RETRIEVAL METHODS

### 2.1. In-situ soil moisture

Contemporary in-situ measurements are relied on as a major source of soil moisture data at a point, either directly in the field (automated methods) or in the laboratory e.g. with gravimetric method. In-situ data is reliable for validating satellite-derived soil moisture estimates because they are accurate. However, in-situ measurements still have a limitation in spatial resolution, areal coverage and representation. In order to acquire a spatial soil moisture map over a heterogeneous area using in situ techniques, interpolation of many soil moisture station data will be required. This is an expensive and time consuming process (Wood, Lin, Troch, Mancini, & Jackson, 1995). Another problem is the calibration and field installation of the instrument; if not properly done can also affect the in-situ soil moisture measurements results. Neutron scattering, gamma ray attenuation, soil electrical conductivity, tensiometry and hygrometry are some of the automated field techniques (Walker, Willgoose, & Kalma, 2004).

### 2.2. Microwave remote sensing of soil moisture

Microwave remote sensing of soil moisture is not affected by suspended materials in the atmosphere like clouds, haze, rainfall and aerosols which interfere with shorter wavelengths (Engman & Chauhan, 1995). The most applied bands in remote sensing are the longer wavelengths L-band, C-band and the short wavelength X-band (Ulaby et al., 1982; Kornelsen & Coulibaly, 2013). It is further subdivided into passive and active microwave sensing of soil moisture (Ulaby et al., 1982). Passive microwave remote sensing instruments measure self emission of the Earth's surface thus depend on the energy from the sun. These satellite sensors have a high temporal resolution but low spatial resolution of up to several kilometres (Ulaby et al., 1982).

Active microwave remote sensing sensors measure the energy that is scattered back by the Earth's surface. These instruments send electromagnetic waves to the Earth's surface and record the amount of radiation scattered back at the same point where the waves were originally transmitted (Ulaby et al., 1982). The quantity measured by active microwave remote sensing instruments is the backscatter coefficient; the unit of measure is decibel (dB).

There are two types of active microwave remote sensing techniques commonly used in soil moisture mapping, categorised as (a) non imaging radar (scatterometers) e.g. wind scatterometers, which are primarily used for measuring wind fields on the oceans with very low resolution of up to tens of kilometres, but can also be used for soil moisture assessment over land and (b) imaging radars e.g. synthetic aperture radar (SAR) which uses synthetic measuring technique to construct high resolution backscatter images. These microwave instruments are light independent thus can work day and night to measure the backscattered energy by Earth's surface. SAR images have a high spatial resolution up to a few metres which makes them costly even though they have a coarser temporal resolution.

Various techniques have been put in place to derive soil moisture from SAR data they include empirical, semi-empirical models and physically based models.

Empirical scattering methods are only valid for the study area for which they have been developed, thus suits one study area. For example linear regression has demonstrated a clear relationship between backscattering coefficient and soil moisture content. This method is simple, as it assumes no change in vegetation and surface roughness over image acquisitions (Petropoulos, 2014). However, care must be

taken, as this method is only valid with the time and data sets used. In addition they require many field measurements hence large dataset to process.

Semi-empirical methods are in between physically based methods and empirical method. These are methods are not site dependent and use little roughness information sometimes even none, for example Oh et al (1992).

Physical models reproduce radar backscatter from soil dielectric constant and surface roughness from a known area. Integral Equation Method (IEM) is an example of physical model, this method however is too complex (Petropoulos, 2014; Van der Velde et al., 2012) as it requires surface roughness information which is hard to obtain due to the dynamic nature of natural surfaces. IEM also neglects subsurface soil volume which is important for dry soil and long wavelength (R. Van der Velde et al., 2014).

Soil moisture can also be estimated using combined passive and active microwave observations. This method utilizes the complimentary parts of both passive and active microwaves. Soil moisture estimates from this techniques is quite accurate. Recently SMAP satellite was launched to offer passive-active soil moisture products.

Microwave remote sensing is the only technique capable of monitoring soil moisture day and night and it is independent of cloud cover. In this regard, soil moisture from microwave remote sensing gives more precise results than from optical region. This has led to the growing interest of soil moisture estimation using remotely sensed imagery (SAR) due to its spatial coverage and high spatial resolution (Van der Velde et al., 2012).

### **2.3. Soil dielectric properties**

Dielectric properties or electric permittivity is a measure of electromagnetic density of an object and indicative for the strength of the reflection (Ulaby et al., 1982). Microwave soil moisture techniques are based upon the different dielectric properties of liquid water ( $\epsilon \approx 80$ ) and dry soil ( $\epsilon \approx 4$ ) (Bindlish & Barros, 2000; Ulaby, Moore, & Fung, 1982; Petropoulos, 2014). Soil texture distribution also affects the soil dielectric behaviour in relation to the amount of free water. Sandy soils have a higher backscatter correlation because of the relatively freely moving water in the large pore spaces, while in clay soil, water is adsorbed onto the soil particle. This makes the water molecules immobile, hence low interaction of radar with bound water (T.Schmugge & Jackson, 1993). In an ideal situation, backscattering coefficient increases with increasing soil moisture until the saturation point. At this point radar backscatter is not sensitive to soil moisture (Kornelsen & Coulibaly, 2013).

Radar signal can penetrate to a certain depth of land surface depending on the wavelength and soil moisture volume, penetration is high in dry soil (Kornelsen & Coulibaly, 2013). Thus scientific studies have been done using SAR in soil moisture retrieval at different frequencies (Bindlish & Barros, 2000; Dubois, van Zyl, & Engman, 1995; Kornelsen & Coulibaly, 2013; R. Van der Velde et al., 2014).

### **2.4. Impact of vegetation on radar backscatter**

Often vegetation affects radar backscatter in a similar manner as soil. Variation of backscatter is influenced by leaf or trunk water content and the vegetation structure, including leaf physiology (Ulaby et al., 1982; Kornelsen & Coulibaly, 2013). Vegetation canopy leads to volume scattering. The penetration depth is influenced by the radar frequency as well as vegetation morphology. Vegetation trunk, branches and stalks have direct backscattering, trunk-soil double scattering and volume scattering (Ulaby et al., 1982).

L-band is the ideal frequency for soil moisture monitoring, as it is water absorption band, in addition it has a higher penetration capability to vegetation. However, double bounce (ground-trunk) is more pronounced (Kornelsen & Coulibaly, 2013). X band has much less penetration capability to vegetation volume. Although C-band has low penetration to vegetation canopy, it is quite sensitive to soil moisture at high biomass, it is this sensitivity to vegetation effect that makes it suitable for the removal of vegetation effect (Kornelsen & Coulibaly, 2013).

The type and shape of land surface feature influences the direction of scattering. When incident energy reaches the surface of the earth it can be scattered, absorbed and reflected as in Figure 2. Depending on the antenna the direction of the backscatter can be horizontal (H) or vertical (V). When the backscatter is returned in the same direction as incident energy we get co-polarization as HH or VV and as cross-polarized HV or VH if the incident energy changes direction as backscatter. Backscatter from the Earth's surface is affected by configuration of the radar instrument, soil and vegetation cover.

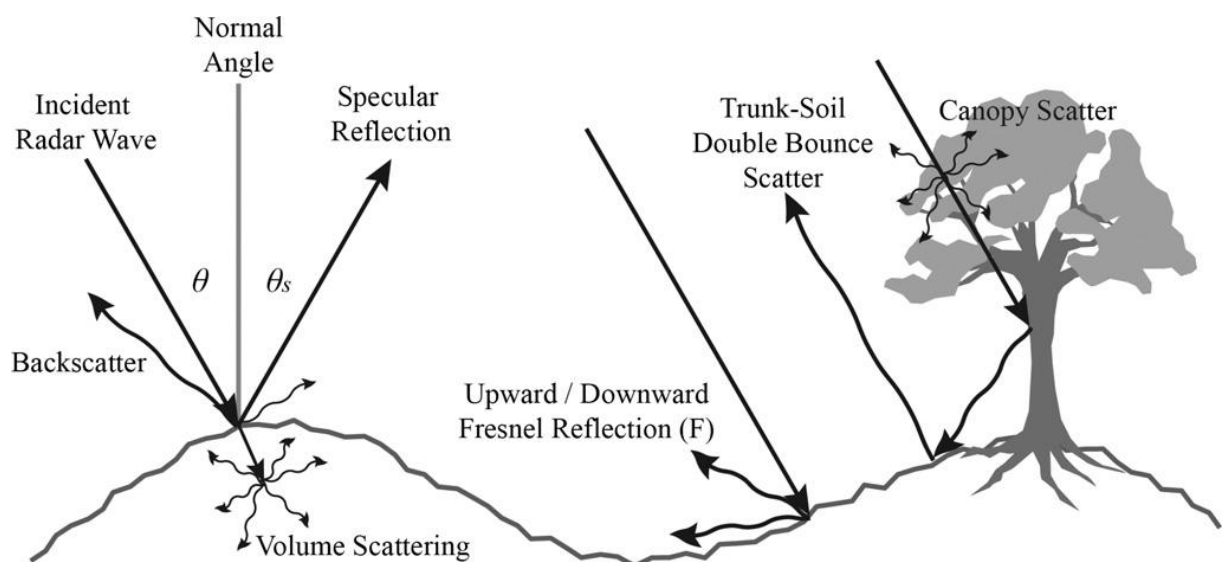


Figure 2: Scattering of an incident radar signal by a rough and vegetated surface. Adapted from (Kornelsen & Coulibaly, 2013).

Increased biomass lowers backscatter sensitivity to soil properties, in this situation, radar backscatter is the sum of the vegetation and soil contribution. As vegetation and surface roughness increases, specular reflection decreases while surface scattering increases leading to increased backscatter (Ulaby et al., 1982). Changes and variations of the vegetation are key item in soil moisture retrieval. It is this dynamism in vegetation that makes the accuracy of its measurement a limiting factor in the accuracy of satellite based soil moisture retrieval (Kornelsen & Coulibaly, 2013).

### 3. DESCRIPTION OF THE STUDY AREA

#### 3.1. River Basin

The study area is located within the Mara River Basin (MRB). The basin is located between longitudes 33.88° and 35.91° W and Latitudes -0.33° and -1.98° S. It has an area of 13,750 km<sup>2</sup> (Mango, Melesse, McClain, Gann, & Setegn, 2011). It is a trans-boundary basin shared in 60% by Kenya and in 40% by Tanzania (Fig.3). Its main tributaries are the Amala, Nyangores, Talek, Sand and Engare Engito on the Kenyan side and the Bologonja River on the Tanzanian side. The river flows from its source in Napuiyapi swamp, 3000m above sea level (a.s.l) within the Mau Forest Complex for 365 km into Lake Victoria at Musoma Bay at 1,134m (a.s.l) (WREM International, 2008). Discussion of other variables of the study area is restricted to the Kenyan side.

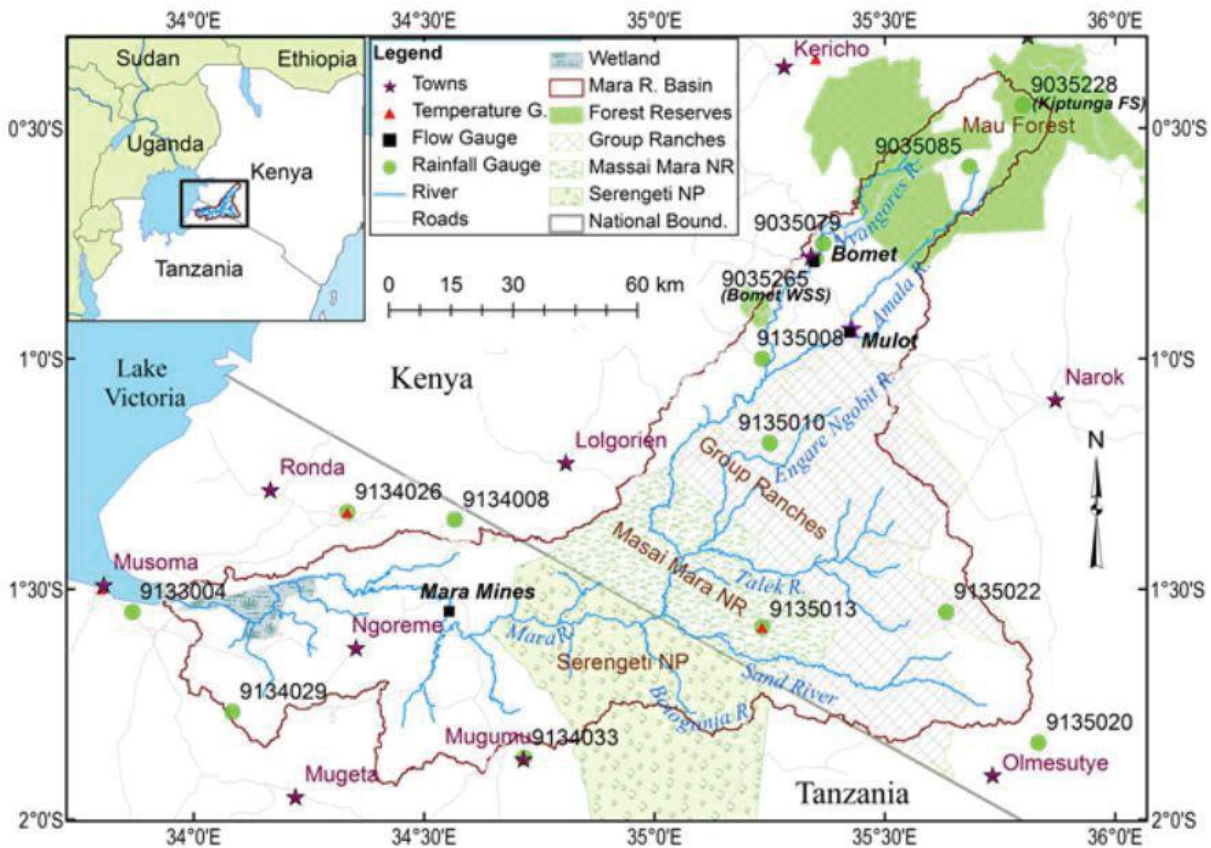


Figure 3: Mara River Basin. (Data source :Dessu et al., 2014).

The catchment includes 1,530 km<sup>2</sup> Masai Mara National Reserve. Around the reserve are group ranches that are either owned by a group of families, or owned by individuals. The ranches include Lemek, Siana and Koyiak. These group ranches cover approximately 4,000 km<sup>2</sup> and are known to be wildlife dispersal areas or dispersal corridors (Bhola, Ogutu, Said, Piepho, & Olff, 2012). The main function of dispersal areas is to connect at least two habitats and reduce the effects of habitat fragmentation, often these regions are prohibited from human development (Bond, 2003). Unlike all the other national parks and reserves in Kenya that are managed by the Kenya Wildlife Service (KWS), the Masai Mara National Reserve is managed by the Narok and Transmara county councils and owned by the Government of Kenya (Ogutu, Owen-Smith, Piepho, & Said, 2011).

This ecosystem has got one of the richest wildlife collections in the world, supporting about 237 herbivores per square kilometre, and its annual wildebeest migrations make it one of the highest visited reserves in the East African region (Waithaka, 2004).

### 3.2. Hydrometeorology

The highlands have cooler temperature, which tend to gradually increase southwards. The mean annual temperature is about 25.5<sup>0</sup> C. Two rainy seasons characterize the rainfall pattern in a year. The long rainy season is from March to June, while the short rainy season typically occurs in November and December. Mean annual rainfall varies from 1750 mm to 300 mm from the upper to the lower part of the basin (Dessu et al., 2014).

### 3.3. Topography and soil

The basin is bounded by the Soit Ooloo escarpment on the west, and the Loita plains and Sannia plains on the east. The altitude ranges between 3044 m (a.s.l) around Mau Forest ecosystem and around 1165m (a.s.l) in Musoma region (refer Fig.1). Figure 4 show the shaded elevation model of the Mara River basin (Ottichilo et al., 2000).

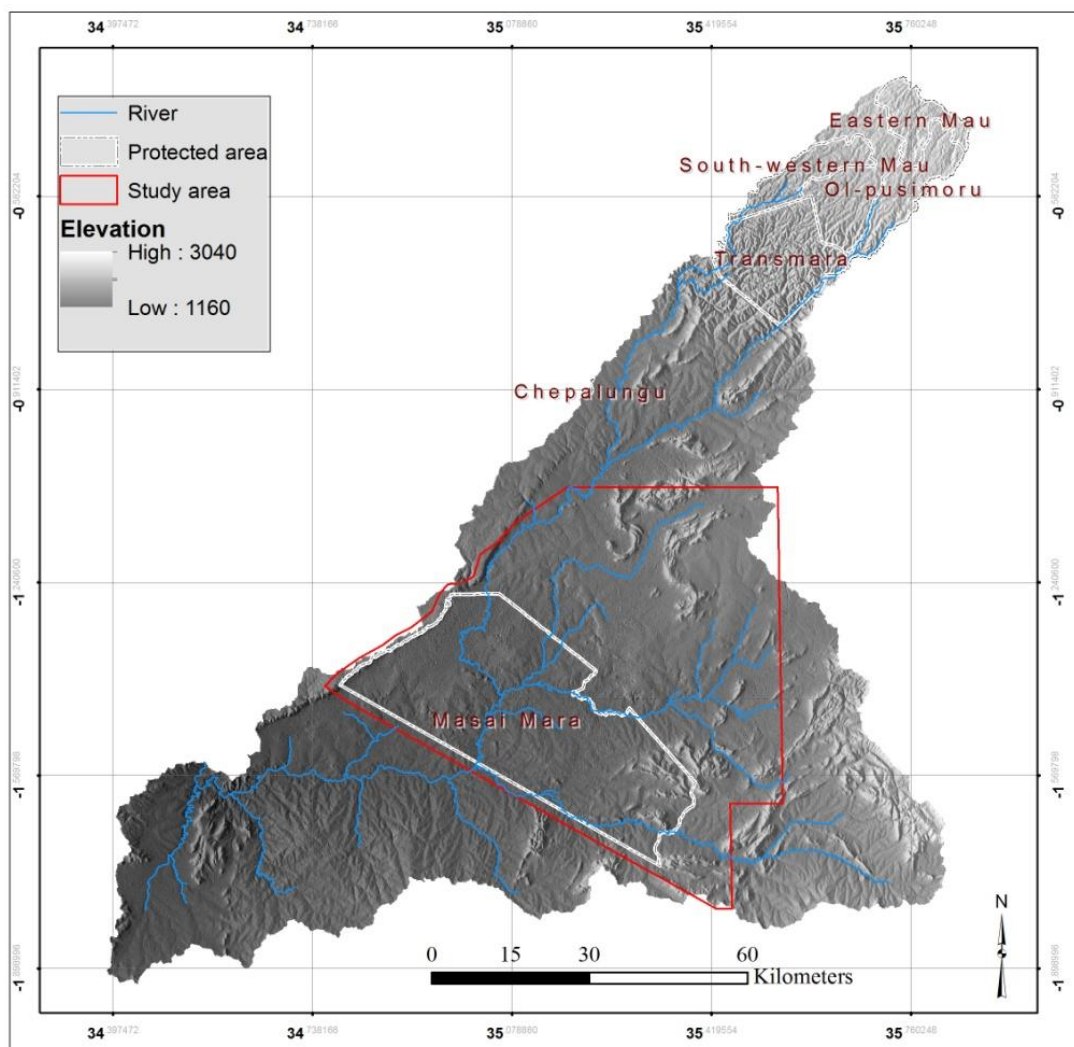


Figure 4: Topography of Mara River Basin (Source: ITC database).

The Mara River Basin is composed of cambisols and vertisols (Mati et al., 2008) as the main soil types. Phonolitic tuffs derived from volcanic ash have been found to be the parent rock in this area (Lamprey & Reid, 2004). Cambisols have a stable structure, highly porous, have good water retention capacity and fairly fertile, thus suitable for agricultural activities. Vertisols are dark with high levels of clay. The underlying bedrock of the region consists of quartzite, gneisses and schist (Lamprey & Reid, 2004). Figure 5 show a description of soil texture of Mara River basin.

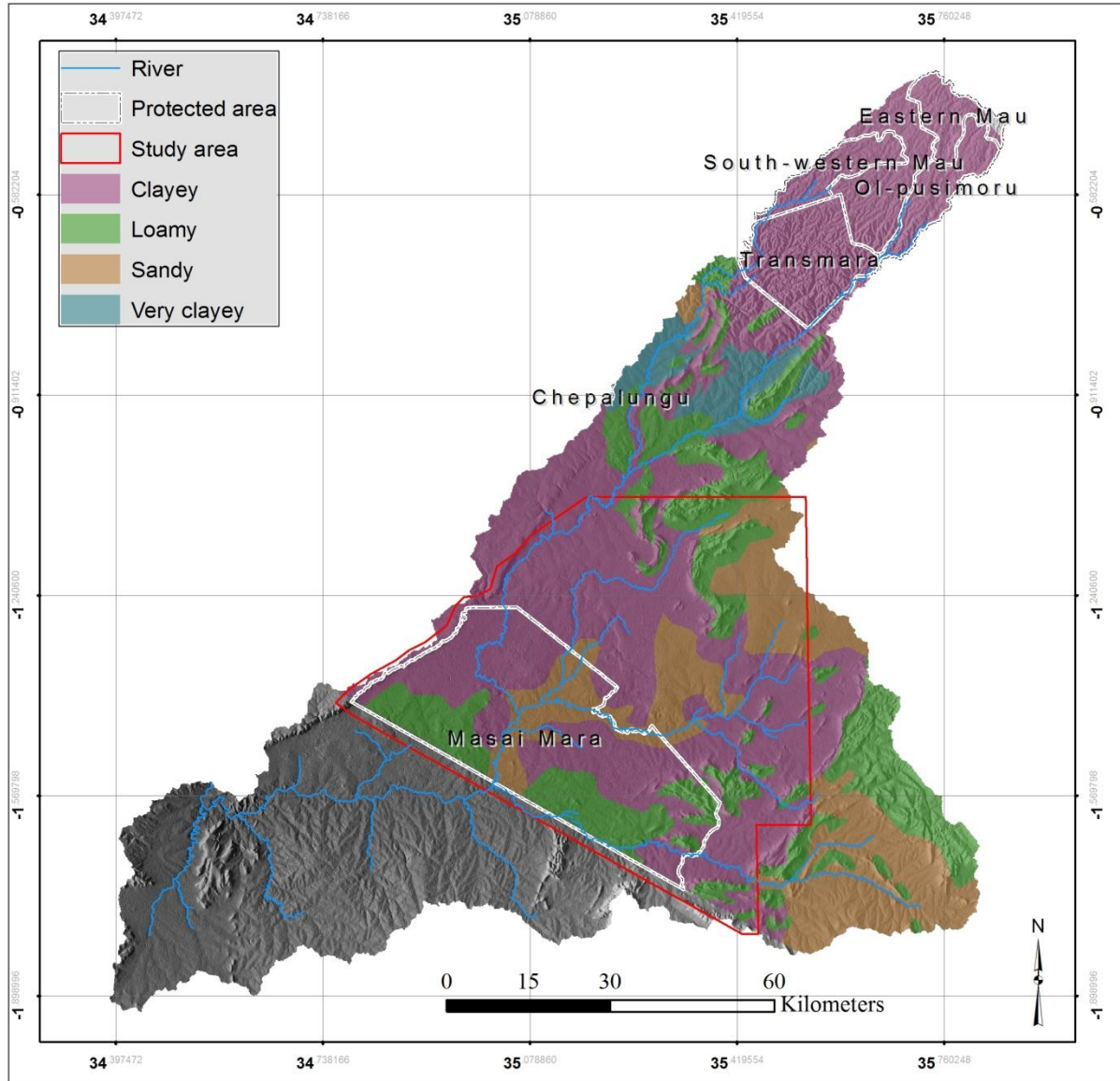


Figure 5: Soil texture within the Mara River Basin (Data source: ILRI).

### 3.4. Socio-economic activities

The main land use/cover types in the Mara River Basin are rangelands comprising of savannah grassland, and shrubland (Bushland) commonly used for grazing (Mati et al., 2008), agricultural activities are predominantly occupied with cash crops like tea and subsistence crops like wheat and maize. Forested areas are concentrated on the higher altitude regions. Figure 6 is a land cover/use map of Mara River Basin section on the Kenyan side.

Land use is restricted to wildlife conservation and tourism within the reserve. However, in the group ranches there is mixed land use, characterised by traditional pastoralism, agriculture (subsistence and commercial), and settlements (Waithaka, 2004). Additionally, these ranches host year round resident wildlife, and also migrant wildlife which spill into them during the dry season (Ottichilo et al., 2000). Group ranches are collection of large tracts of privately owned land for wildlife or livestock rearing.

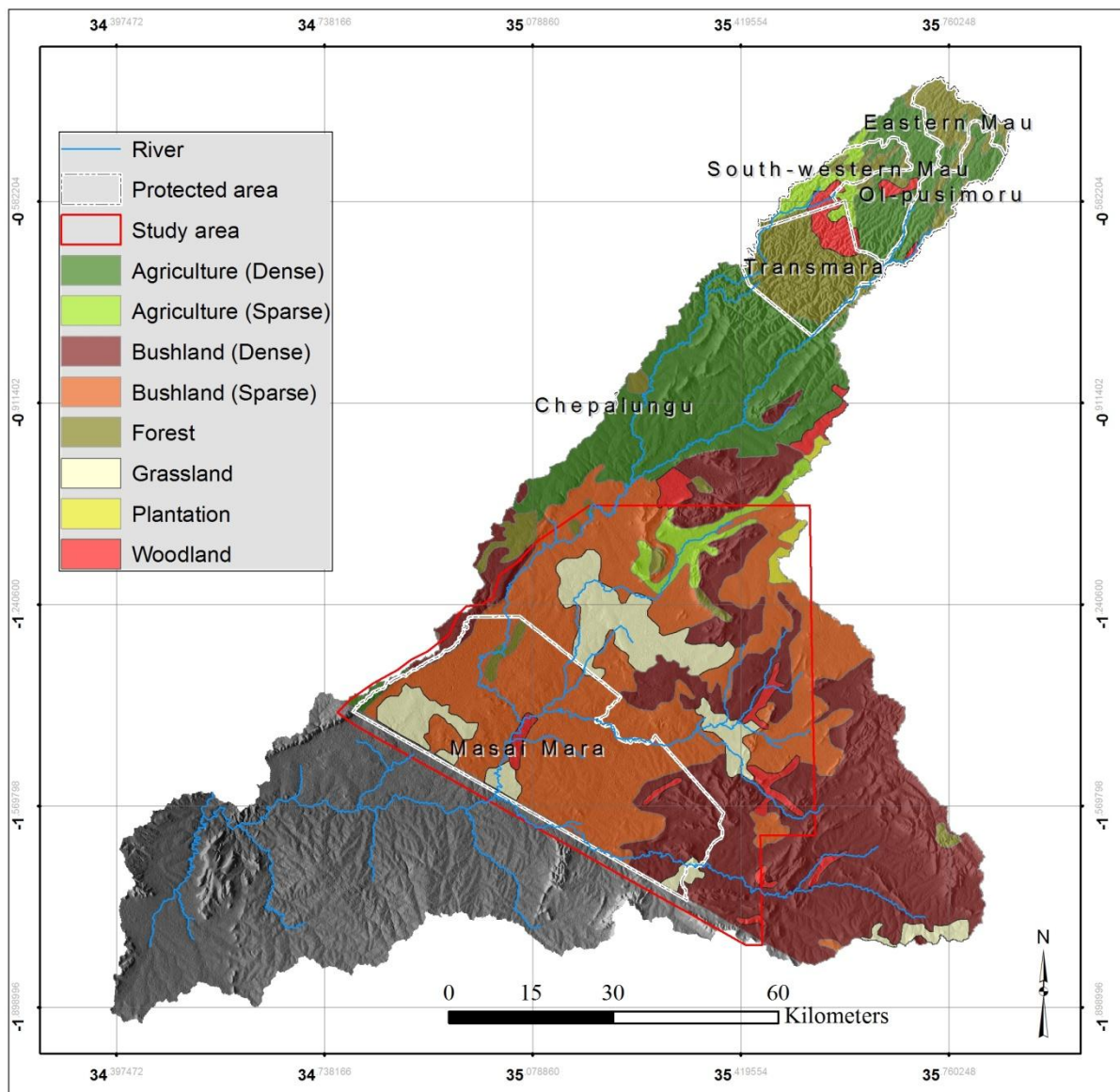


Figure 6: Land cover classes within the Mara basin ecosystem (Data source: ILRI).

## 4. IN SITU DATA

### 4.1. Kenya Mara Soil Moisture Station

For the development of the soil moisture monitoring network, a preliminary selection of suitable soil moisture monitoring sites was based on the time series analysis of 14 years of 250 m resolution MODIS NDVI imagery analysed by Dr. Kees de bie. A detailed field report on the installation was compiled by Dr. Rogier van der Velde. The NDVI was chosen for the determination of the measurement location, as the primary purpose of the network was to support the understanding of vegetation growth in response to rain. The objective in this context was to cover a broad range of vegetation growth conditions that was determined by hydrology (as a function of soil type) and meteorology (e.g. rain, evaporative demand). It was expected that with the six stations regional scale variability can be captured although this network would be too sparse for capturing the local variations.

The following statistics were deduced from the MODIS NDVI data set: i) median, ii) standard deviation and iii) the trend. The trend here was taken as the slope of a linear equation ( $NDVI_{est} = a t + b$ ) fitting through the MODIS NDVI data points. An unsupervised classification was performed using these three statistical parameters after which the study area was segmented into polygons with ‘uniform’ statistical NDVI properties. Figure 7 shows a topographic map of the Masai Mara reserve and the surrounding conservancies overlain with polygons indicating the areas with ‘uniform’ long-term NDVI statistics.

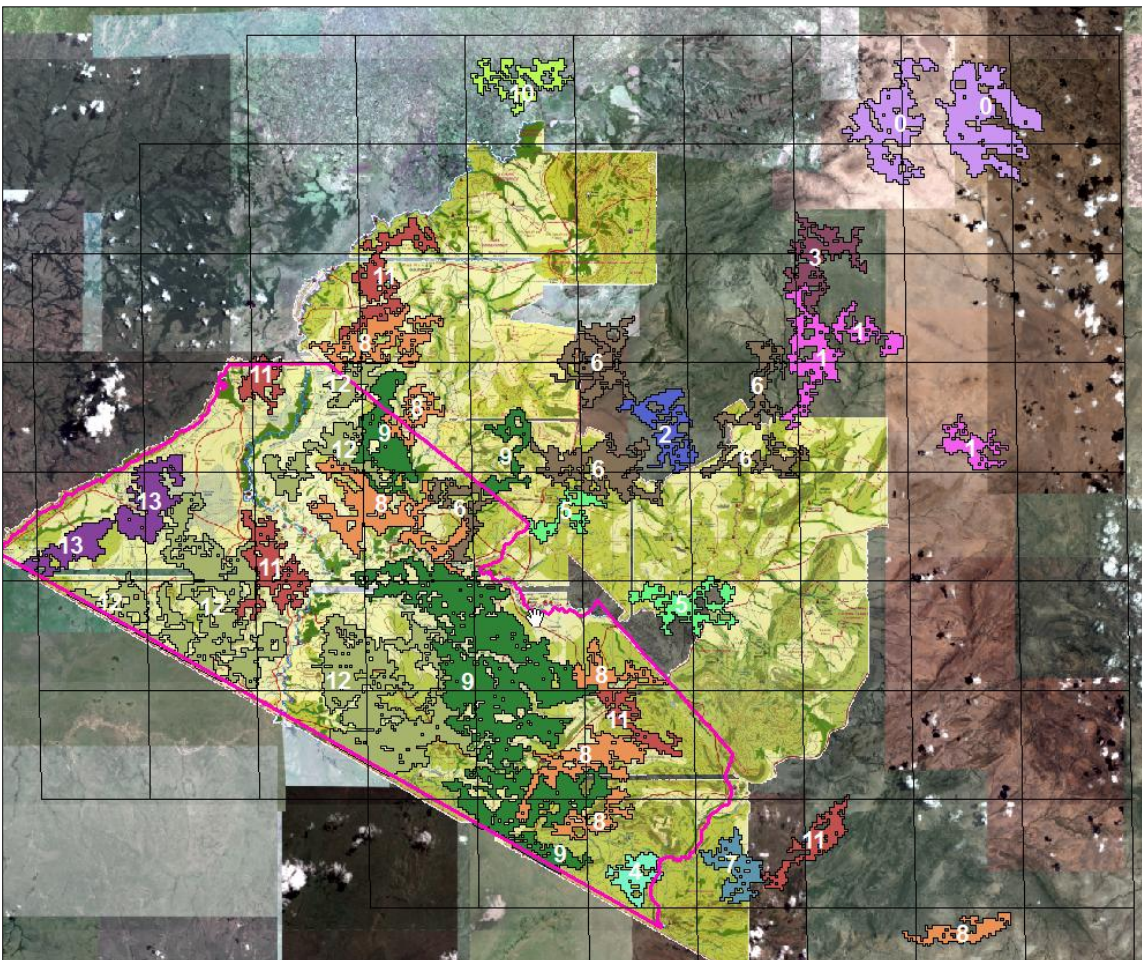


Figure 7: Topographic map of the Masai Mara reserve (Purple boundaries) and surrounding conservancies on top of which polygons are shown of areas that have fairly uniform statistics properties deduced from a 14 year long time series of MODIS NDVI (Courtesy Kees de bie)

Table 1 provides the statistics (median, stdev, size of the area), description of the location and motivation for (not) sampling in this area, whereby the listed ID number correspond to the number in the map (Figure 7). It should be noted that the numbers given for the median and stdev NDVI is an ID number and does not represent the actual value, but low values are low NDVI (biomass) and high values are high NDVI (biomass).

As preliminary distribution of the monitoring sites, two were predestined for the reserve and the remaining four for installation in the conservancy. Polygons with ID9 and ID12 were selected for the reserve as these represent the largest portions of the reserve and have distinct median NDVI, which is typically higher than in the conservancy. Outside the reserve polygons with ID5, 6, 7 and on one of ID1, 2, and 3 were selected: i) #5 and #6 were selected as a good representation for medium biomass conditions in the study area (reserve + conservancy), whereby area #5 displays a decreasing NDVI trend; ii) #7 was selected to increase the spatial coverage of the network; iii) #1, #2, or #3 were selected as a good representation for low biomass conditions in the conservancy. Instructions were to select a site for the practical issues regarding the installation (e.g. accessibility to ease maintenance, security issues, mobile phone reception for near real-time communication).

Table 1: Description of the polygons shown in figure 10 representing the largest areas with each uniform long-term NDVI statistics (i.e. median, standard deviation) deduced from a 14 years MODIS NDVI data set. The colours correspond to argumentation for (not) sampling.

ID	Description location	median	stdev	Area	Argumentation for (not) sampling
		-	-	km <sup>2</sup>	
0	agriculture	10	6	89.4	Not relevant LC type
1	neither conservancy nor reserve	11	4	47.4	One of these seems appropriate as a representation of the rangelands outside the conservancies/reserve
2	neither conservancy nor reserve	12	4	20.1	
3	neither conservancy nor reserve	12	5	23.2	
4	reserve	13	3	11.6	Too small area in the reserve
5	conservancy	13	4	29.7	1. Yes, area in conservancy with detected degradation (not shown here)
6	conservancy	13	4	97.2	2. Yes, large area in conservancy
7	conservancy	14	3	16.0	Possibly, good range from east to west, question is whether this actually a conservancy
8	reserve/conservancy	14	4	143.3	Too fragmented across the study area questionable whether this is a physically existing unit
9	reserve/conservancy (small)	14	5	237.7	Yes, representative for reserve
10	outside study area	15	3	17.2	Outside SA
11	reserve/conservancy (small)	15	4	90.1	Too fragmented across the study area questionable whether this is a physically existing unit
12	reserve	15	5	228.6	Yes, representative for reserve
13	reserve	16	5	43.7	Too high biomass, not representative reserve

## 4.2. The network

The monitoring network was established starting from September 23<sup>rd</sup> up to September 28<sup>th</sup>. The stations are named KMSTXX which stands for Kenya Mara Station (KMST) with XX as the ID number. KMST01 and KMST02 are installed in the reserve, and KMST03, KMST04, KMST05, and KMST06 are installed in the conservancy. Table 2 lists the stations' short descriptions, geographic information (Latitude, Longitude in WSG84) along with the ID of the polygon in Fig. 7 for which the station is representative. Figure 8 shows the location of the six stations with a Landsat 5 TM false colour composite in the background that covers the study area, while figure 9 shows the photographs of each station location.

The instrumentation consists of Decagon EM50G (wireless) data loggers and 5TM probes for measuring soil moisture as well as soil temperature. Specific details about this equipment can be found at <http://www.decagon.com>. Each station was equipped with a data logger and five probes inserted vertically with the centre pin at nominal soil depths of 5, 10, 20, 40 and 80 cm. Upon installation, the data loggers were programmed to store a set of readings every 15 minute. The stations form a base for the ongoing MaMaSe project as its soil moisture monitoring network.

Table 2: List of monitoring stations installed in the Masai Mara Reserve and surrounding conservancies whereby the ID number corresponds to the polygons in Fig. 7.

Station	Description	ID number	Date	Latitude	Longitude	Elevation
KMST01	Reserve	12	23/9/2014	1.32043° S	35.03639° E	1550 m
KMST02	Reserve	9	24/9/2014	1.51988° S	35.16982° E	1591 m
KMST03	Conservancy	7	25/9/2014	1.66166° S	35.43250° E	1840 m
KMST04	Conservancy	1,2,3	26/9/2014	1.20499° S	35.46390° E	1908 m
KMST05	Conservancy	5	27/9/2014	1.45698° S	35.38197° E	1709 m
KMST06	Conservancy	6	28/9/2014	1.23306° S	35.25944° E	1752 m

\*coordinates in Lat/Lon WSG84

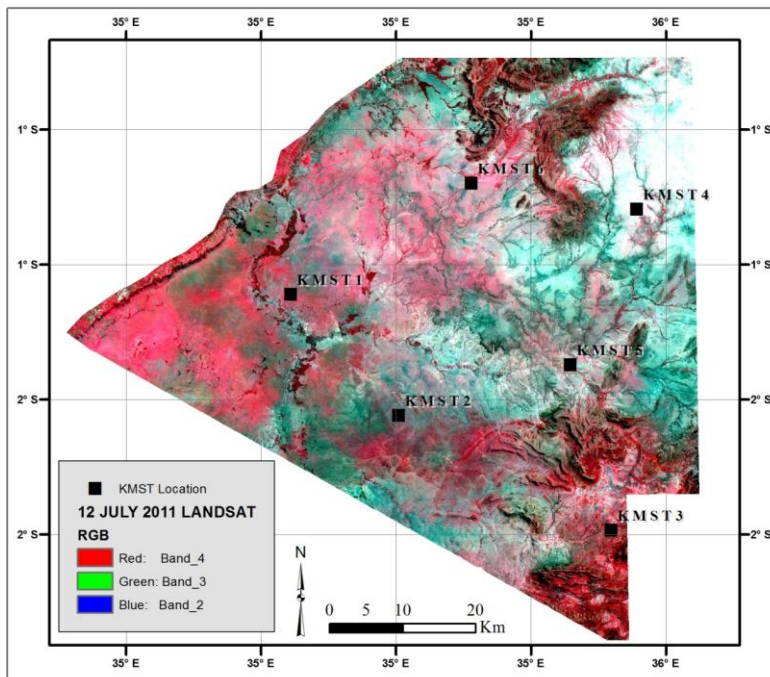


Figure 8: False colour composite (R: band4, G: band3, B: band2) of a Landsat 5TM acquisition taken on 12 July 2011 indicating the location of the soil moisture monitoring stations.

A detailed description of each location where each station was installed is given in Appendix 1, including the date, soil type, land cover and topography.



Figure 9: General landscape locations of KMST

#### 4.3. Calibration

For calibration of the probes, soil samples of approximately 10 kg from each of the six stations was packed in 30 litre box in the field, of which 5-6 kg of soil was repacked into smaller 12 litre bucket for calibration. The following procedure was adopted (Rogier van der Velde, Eweys, Nyang'acha, Gathecha, & Vekerdy, 2014)

- Soil was air dried;
- 5 kg of soil was repacked into 12 liter bucket;
- simultaneous probe reading and soil samples were taken after adding about 100 ml of water into the soil sample, 100 ml of water was added and carefully mixing the soil. It was found that the probes were sensitive to bulk density. The soil was therefore compacted after adding water;
- The soil samples were weighed and dried in the oven at 105° C for 24 hours;
- the wet and dry weight were used to calculate the volumetric soil moisture using;

$$\theta = \frac{m_{wet} - m_{dry}}{V_{soil}} \quad (1)$$

Where  $\theta$  is the volumetric soil moisture content ( $m^3 m^{-3}$ ),  $m_{wet}$  is the mass of the wet soil (kg),  $m_{dry}$  is the mass of dry soil (kg) and  $V_{soil}$  is the volume of dry soil ( $m^3$ ) computed as;

$$V_{soil} = \frac{m_{dry}}{\rho_{bulk}} \quad (2)$$

Where,  $\rho_{bulk}$  is the bulk density ( $Kg m^{-3}$ );

The probe readings and gravimetrically determined volumetric soil moisture contents (VSM) collected under various wetness conditions were used to develop a soil specific calibration. A difference was noted in probe response for KMST02 and KMST 03 and the other stations (KMST01, KMST04, KMST05 and KMST06) (Fig.10). Two matchup sets were defined and for each a calibration function developed.

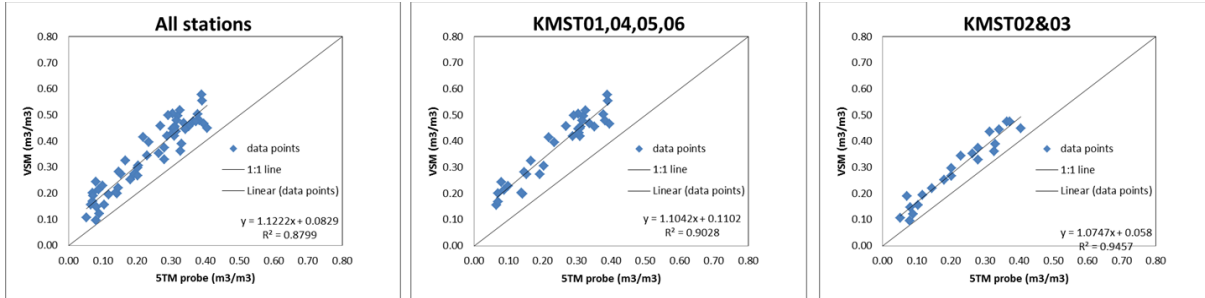


Figure 10: Probe soil moisture plotted against gravimetric soil moisture content, (A) all stations, (B) KMST01, 04, 05 and 06, (C) KMST02 and 03 (Rogier van der Velde et al., 2014).

It was also noted that the measured response of the probes to soil moisture was linear, thus the relationship for calibrating the probe soil moisture into volumetric soil moisture is taken in the form of ( $\theta$  in  $\text{m}^3 \text{m}^{-3}$ ),

$$\theta = a \theta_{5TM} + b \quad (3)$$

Where  $\theta_{5TM}$  is the probe reading ( $\text{m}^3 \text{m}^{-3}$ ) and **a**, and **b** are fitting parameters.

The linear functions were fitted through the data points shown in Figure 10. Table 3 provides the fitting parameters with the associated error statistics. The error statistics are in agreement with the ‘state-of-the-art’ (e.g. RMSD  $\sim 0.045 \text{ m}^3 \text{ m}^{-3}$ ) even when treating all stations equally. However, the reliability of the calibration is improved by  $> 20\%$  if a distinction is made between stations KMST02&03 and the other stations resulting in a RMSD of  $0.035 \text{ m}^3 \text{ m}^{-3}$ .

Table 3: Calibration parameters for the decagon 5TM probe installed in the Masai Mara reserve and conservancy with associated error statistics.

Soil Type	Parameters		Error statistics		
	a	b	R <sup>2</sup>	RMSD ( $\text{m}^3 \text{m}^{-3}$ )	MAD ( $\text{m}^3 \text{m}^{-3}$ )
Generic	1.1222	0.0829	0.880	0.045	0.037
KMST01*	1.1042	0.1102	0.928	0.035	0.028
KMST02**	1.0747	0.0580			

\* KMST01 represents also stations KMST04, 05 & 06.

\*\* KMST02 represents also station KMST02

#### 4.4. Organic matter determination

Organic matter analysis was done to determine the organic content of the soil. This is the ratio in percentage of the mass of organic matter in a measured mass of soil to the mass of the dry solid soil. Organic matter plays an important role in biological, physical and chemical properties of soil, as well as retention and the rate of vertical water movement. The organic matter determination was done for each of the six stations. The procedure can be found in Appendix 2. This was done to aide in particle size analysis.

#### 4.5. Particle size analysis

Soil sample was taken at each station at random depth just below the root zone, this was done with an assumption that the soil profile did not change in the 80cm depth. The samples were weighed and dried for soil moisture analysis and calibration of the KMST data loggers. In addition the disturbed soil samples were used for soil texture analysis at the ITC laboratory. The procedure carried out for the soil texture analysis is as follows:

- Add around 20g soil for each samples in the beakers with labels;
- Add the mixed solution (H<sub>2</sub>O<sub>2</sub> and water, H<sub>2</sub>O<sub>2</sub>: Water = 1:2) to each beaker and cover with a watch glass; let the mixture stand overnight.
- place beaker on water bath at 80°C with regular addition of H<sub>2</sub>O<sub>2</sub> until decomposition of organic matter
- add water to a volume of about 300 ml
- place on hot plate to boil till there are no bubbles (but not dry), which means that the organic matter is removed;
- Cool the beakers on a slight angle, allow to settle and siphon off
- Add the mixed solution (HCL and water, HCL :Water =1:2) to the beakers with organics removed for removing the calcium, wait till there are no bubbles anymore;
- the mixture was transferred to a wash bottle, capped and shaken on an end over end shaker overnight at speed of 30 rpm
- Pass the suspension through a 50µm sieve placed above sedimentation cylinder.
- Make to 1 liter mark
- For >50µm material this was collected during sieving
- for <50µm after measuring the temperature of the suspension, shake well, after 1 minute pipette 20ml at a depth (cm) of 11.2
- For <20µm after measuring the temperature of the suspension, shake well, after 5 minutes pipette 20ml at a depth (cm) of 9.7
- For <2µm after measuring the temperature of the suspension, shake well, after 5 1/2 hours pipette 20ml at a depth (cm) of 6.4
- put the measured aliquot in oven overnight at 105°C
- Cool in a desiccator and weigh using precision scale
- for the material >50µm after drying, transfer to the top sieve of a stacked set of sieves on the following mesh sizes; >1mm,0.5mm,0.25mm,0.1mm,0.56mm
- sieve for 10 min on the sieving machine at amplitude 7.0 and interval 4
- empty each sieve into a measured cup and weigh on a precision scale

According to the United States Department of Agriculture (USDA) soil texture classification with Clay as particles less than 2 µm, Silt as 2 – 50 µm particles and Sand as particles greater than 50 µm.

The proportional amount of individual fractions was calculated as equation 4:

$$\% \text{clay, silt, sand} = \frac{\text{individual fraction}}{\text{sample weight}} \times 100 \quad (4)$$

In order to obtain each fraction as a function of the total soil then, equation 5 was applied:

$$\% \text{clay, silt, sand of total soil} = \frac{100 - \%(\text{fraction} > 2\text{mm} + \text{organic matter})}{100} \times \% \text{ clay, silt, sand of fine earth} \quad (5)$$

Figure 11 shows, the particle size distribution of each station. KMST01 was found out to be having high levels of clay soil. The particle size distribution was expected since the area selected was large. Table 4 is showing the types of soil according to the USDA classification.

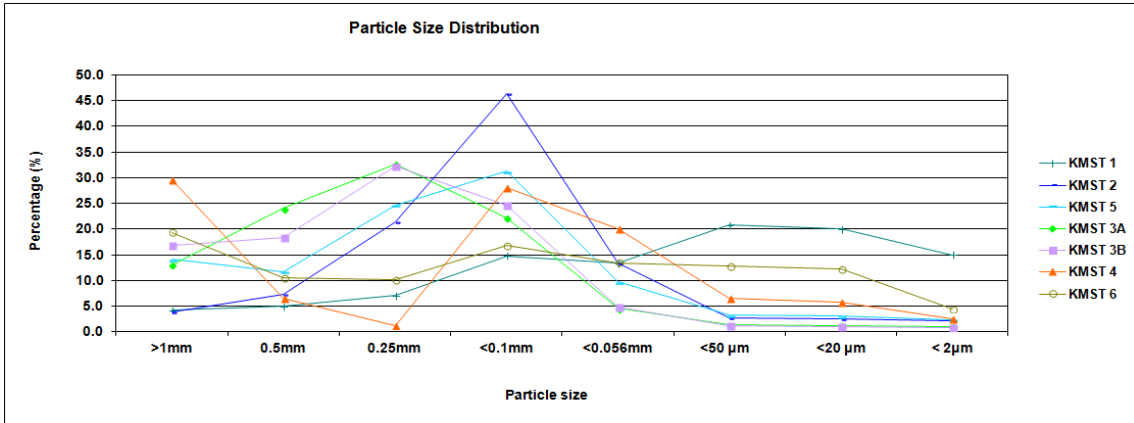


Figure 11: Particle size distribution of the location each KMST.

Table 4: Soil texture (Clay, Silt, and Sand) for the five Mara stations installed in 2014.

	SAND	SILT	CLAY	Soil Type
	>50µm	2µm - 50µm	< 2µm	
<b>KMST 1</b>	44.26	40.77	14.97	Loam
<b>KMST 2</b>	92.55	5.33	2.12	Sand
<b>KMST 5</b>	91.39	6.29	2.33	Sand
<b>KMST 3A</b>	96.35	2.57	1.08	Sand
<b>KMST 3B</b>	96.88	2.22	0.90	Sand
<b>KMST 4</b>	85.26	12.19	2.55	Loamy sand
<b>KMST 6</b>	70.35	25.17	4.47	Sandy loam

## 5. SATELLITE DATA

### 5.1. Tropical Rainfall Measuring Mission (TRMM)

The Tropical Rainfall Measuring Mission (TRMM) is a satellite operated by both NASA and the Japan Aerospace Exploration Agency (JAXA). It is designed to study tropical rainfall. TRMM is designed with five instruments (Figure 12) including Precipitation Radar (active microwave sensor), TRMM Microwave imager (TMI) (passive microwave sensor), Visible and InfraRed Scanners (VIRS) Cloud and Earth Radiant Energy Sensor (CERES) and Lightning Imaging Sensor (LIS).

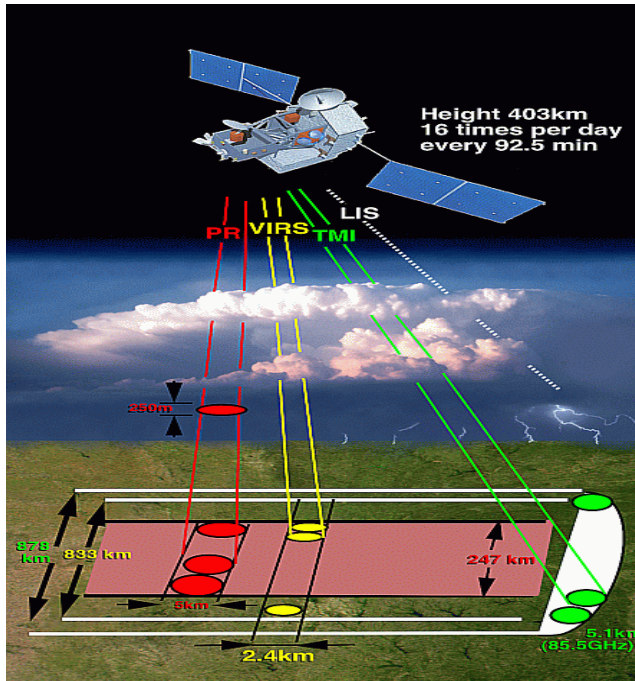


Figure 12: Measurement instruments onboard TRMM satellite (NASA, 2014b).

The Precipitation Radar provides information on storm structure, including the intensity and distribution of the rain, rain type, storm depth and on the height at which the snow melts into rain (NASA, 2014b). The TRMM TMI is the main rain measuring sensor. It is a passive microwave sensor that is used to provide quantitative rainfall information. TRMM TMI is capable of quantifying the water vapour, the cloud water, and the rainfall intensity in the atmosphere. VIRS is used to monitor radiation coming up from the Earth. The intensity of the radiation is used to determine the brightness or temperature of the source (NASA, 2014b). LIS is an instrument that is used for locating lightning over the tropics, this information is important for issuing warning on the state of severe storms (NASA, 2014b).

This research used the TRMM 3B42 version 7 product resampled to daily temporal resolution. The product is a result of the TRMM Multi-Satellite Precipitation Analysis (TMPA) (NASA, 2014b). The data is available on a  $0.25^\circ \times 0.25^\circ$  resolution and at latitudes  $50^\circ$  N and  $50^\circ$  S.

### 5.2. Digital Elevation Model

Shuttle Radar Topographic Mission (SRTM) was a programme between the National Imagery and mapping Agency (NIMA) and the National Aeronautics and Space Administration (NASA) (USGS, 2008). The 11 day space mission was fitted with a radar system composed of two antenna panels, X-band and C-

band, and the main task was to produce digital topographic data. The C-band covered almost the entire globe to produce Digital Elevation Models (DEM), the X-band radar data is used to construct high resolution DEM however it is not covering the entire globe (USGS, 2006). The data can be downloaded from Global Land Cover Facility website (GLCF). A summary of SRTM DEM specification is shown in Table 5. This study used 3 arcs-second SRTM DEM.

Table 5: Summary of SRTM DEM Properties.

Product Specifications	
Projection	Geographic
Horizontal Datum	WGS84
Vertical Datum	EGM96 (Earth Gravitational Model 1996)
Vertical Units	Meters
Spatial Resolution	1 arc-second for the United States (~30 meters)
	3 arc-seconds for global coverage (~90 meters)
Raster Size	90 m

### 5.3. MODIS NDVI

Moderate Resolution Imaging Spectroradiometer (MODIS) is an instrument aboard Terra and Aqua satellites. These satellites were launched in Dec. 18, 1999 as a sun synchronous circular orbit at an altitude of 705km. the angle of inclination is 98.5° and takes 16 orbits per day. The descending nodal crossing is at 10:30 AM (eoportal, 2014). They are managed by NASA and tasked to obtain physical and radiation information from clouds, air-land and air-sea exchange of energy, carbon, and water, in addition to measurement of trace gases.

MODIS sensor main task is to measure biophysical and biochemical processes from vegetated surfaces, this is achieved through the use of Normalized Difference Vegetation Index (NDVI) and Enhanced Vegetation Index (EVI) products.

Normalized Difference Vegetation Index (NDVI) is a widely used index in vegetation studies and monitoring, it is obtained through a ratio of red and near infrared regions of the spectral reflectance as follows;

$$NDVI = \frac{NIR_{(0.86\mu m)} - RED_{(0.67\mu m)}}{NIR_{(0.86\mu m)} + RED_{(0.67\mu m)}} \quad (6)$$

The index is derived from band 1 and 2 of MODIS instrument, obtained from daily, atmosphere-corrected bidirectional surface reflectance (NASA, 2014a). MODIS NDVI is a consistent product that provide spatial and temporal comparison of vegetation canopy greenness, leaf area, chlorophyll, and canopy structure of vegetation (NASA, 2014a).

This study used MYD13Q1 product, the product is the optimized 16-day maximum data at 250-meters spatial resolution, as in Table 6. The root name indicates the product type, year and Julian day of the year, spatial resolution and temporal resolution e.g. The Hierarchical Data Format version 4 (HDF4) is the default file format, and it is available in sinusoidal projection.

Product type	Year and Julian day	Spatial resolution	Temporal resolution
MYD13Q1	A2011_137- 2011_157	250m	16 Days

Eleven (11) MODIS NDVI images that correspond as close as possible to the SAR data dates were provided from ITC database. Also some were downloaded from <http://reverb.echo.nasa.gov>.

Table 6: MODIS NDVI image dates used for the study

	<b>MODIS_NDVI 2011_2012</b>	<b>Julian Day</b>
1	MYD13Q1.A2011137.h21v09.005.2011157005714.250m_16_days_NDVI	137-157
2	MYD13Q1.A2011329.h21v09.005.2011346140517.250m_16_days_NDVI	329-346
3	MYD13Q1.A2011361.h21v09.005.2012013030810.250m_16_days_NDVI	361-013
4	MYD13Q1.A2012009.h21v09.005.2012026032249.250m_16_days_NDVI	009-026
5	MYD13Q1.A2012057.h21v09.005.2012075004120.250m_16_days_NDVI	057-075
6	MYD13Q1.A2012089.h21v09.005.2012108131240.250m_16_days_NDVI	089-108
7	MYD13Q1.A2012105.h21v09.005.2012122050952.250m_16_days_NDVI	105-122
8	MYD13Q1.A2012137.h21v09.005.2012159184029.250m_16_days_NDVI	137-159
9	MYD13Q1.A2012153.h21v09.005.2012170030718.250m_16_days_NDVI	153-170
10	MYD13Q1.A2012185.h21v09.005.2012202131938.250m_16_days_NDVI	185-202
11	MYD13Q1.A2012233.h21v09.005.2012250021748.250m_16_days_NDVI	233-250

**5.4. RADARSAT-2**

RADARSAT-2 (RS2) is a Canadian satellite that was launched in December 14 2007. It is a continuation to RADARSAT-1, which retired on April 2013. The RS2 is a SAR C-band sensor with capabilities of providing high spatial resolution data with single and multiple polarizations. Figure 13 indicates observation geometries and coverage modes of RADARSAT-2 while Table 7 is showing some general properties of RS2 products. The data used for this study was made up of 11 images obtained from 24 May 2011 to August 2012. The dual polarized (VV+VH) wide swath data was obtained as SAR Georeferenced Fine Product (1SGF).

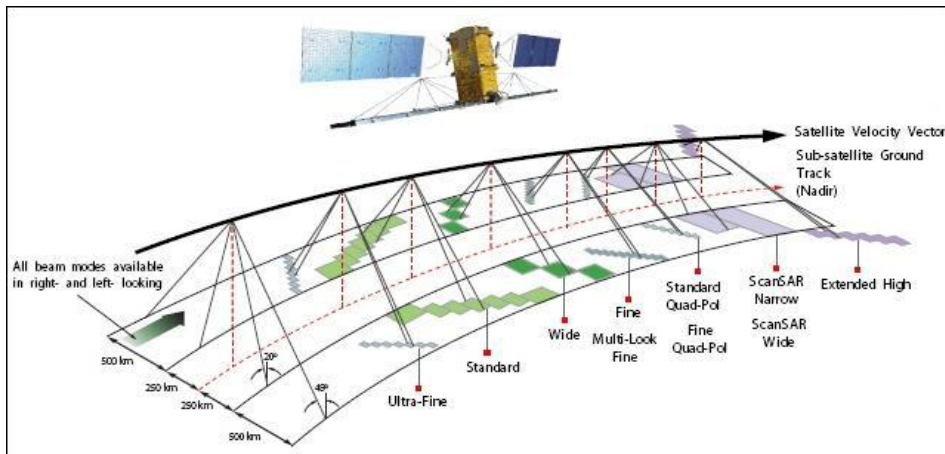


Figure 13: Observation geometries and coverage modes of RADARSAT-2. Image retrieved from (<https://directory.eoportal.org>).

Table 7: Summary of RADARSAT-2 properties

RADARSAT-2 Characteristics	
Active Antenna	C-Band
Centre Frequency	5.405 GHz
Bandwidth	100 MHz
Polarization	HH, VV, HV, VH
Polarization Isolation	> 25 dB
Aperture Length	15 m
Aperture width	1.37 m
Mass	750 kg
Altitude	798 km
Inclination	98,6 degrees
Duration of one orbit	100.7 min
Descending node	6 hrs.
Ascending node	18 hrs.
Sun-synchronous	14 orbits per day

### 5.5. Sentinel-1

Sentinel-1 (S1) is a SAR C- band imaging radar. The Sentinel-1 mission is to provide more frequent revisit time, wider coverage, enhanced timeliness and reliability for operational services and applications that require long time series data (ESA, 2014). It operates in single polarization (HH or VV) and dual polarization as (HH+HV or VV+VH) (Torres et al., 2012). S1 has two satellites, S1A and S1B. The discussion in this study is based on S1A.

Sentinel-1A SAR has four acquisition modes (Figure 14). This research utilized Ground Range Detected High Resolution (GRDH) for Interferometric wide swath (IW). The S1A\_IW\_GRDH products have a spatial resolution of 10 m, and revisit time of 12 days. A Summary of major characteristics of each mode is shown in Table 8.

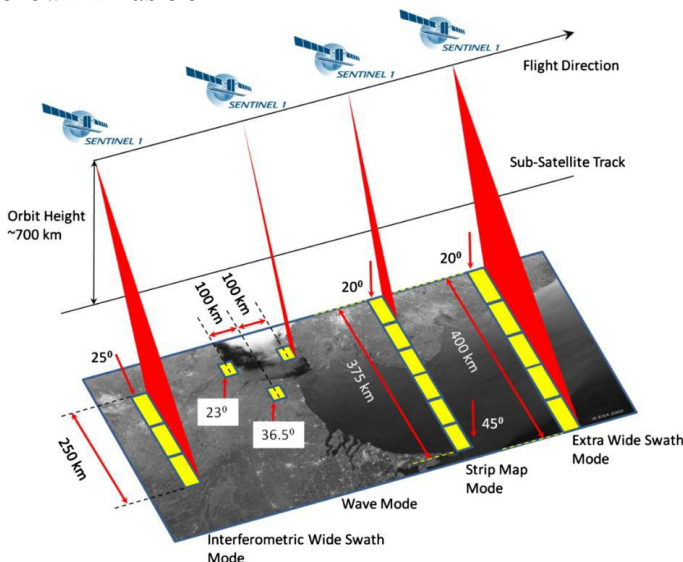


Figure 14: Sentinel-1 image acquisition modes (Source: ESA, 2014)

- Strip map (SM) - A standard SAR strip map imaging mode is where the ground swath is illuminated with a continuous sequence of pulses, while the antenna beam is pointing to a fixed azimuth and elevation angle.
- Interferometric Wide swath (IW) - Data is acquired in three swaths using the Terrain Observation with Progressive Scanning SAR (TOPSAR) imaging technique. In IW mode, bursts are synchronized from pass to pass to ensure the alignment of interferometric pairs. IW is sentinel-1's primary operational mode over land.
- Extra Wide swath (EW) - Data is acquired in five swaths using the TOPSAR imaging technique. EW mode provides very large swath coverage at the expense of spatial resolution.
- Wave (WV) - Data is acquired in small strip map scenes called "vignettes", situated at regular intervals of 100 km along track. The vignettes are acquired by alternating the acquisition one vignette at a near range incidence angle while the next vignette is acquired at a far range incidence angle. WV is sentine-1's operational mode over Open Ocean.(ESA, 2014)

Table 8: Sentinel-1 main acquisition modes, courtesy (Torres et al., 2012).

Parameter	Interferometric Wide-swath mode (IW)	Wave mode (WV)	Strip Map mode (SM)	Extra Wide-swath mode (EW)
Polarisation	Dual (HH + HV, VV + VH)	Single (HH, VV)	Dual (HH + HV, VV + VH)	Dual (HH + HV, VV + VH)
Access (incidence angles)	31°-46°	23°-37° (mid incidence angle)	20°-47°	20°-47°
Azimuth resolution	<20 m	<5 m	<5 m	<40 m
Ground range resolution	<5 m	<5 m	<5 m	<20 m
Azimuth and range looks	Single	Single	Single	Single
Swath	>250 km	Vignette 20 × 20 km	>80 km	>410 km
Maximum NESZ	-22 dB	-22 dB	-22 dB	-22 dB
Radiometric stability	0.5 dB (3σ)	0.5 dB (3σ)	0.5 dB (3σ)	0.5 dB (3σ)
Radiometric accuracy	1 dB (3σ)	1 dB (3σ)	1 dB (3σ)	1 dB (3σ)
Phase error	5°	5°	5°	5°

Sentinel-1 will offer high temporal resolution of up to 6 days when both S1A and S1B are in orbit, large spatial coverage with fast data dissemination. The Sentinel-1 data was downloaded from <https://senthub.esa.int> the available data is shown in Table 9.

Table 9: Sentinel-1 images available

	Sentinel-1A data
1	S1A_IW_GRDH_1SSV_20141028T032002_20141028T032027_003024_003733_7BEC
2	S1A_IW_GRDH_1SSV_20141028T031937_20141028T032002_003024_003733_71B5
3	S1A_IW_GRDH_1SSV_20141121T031937_20141121T032002_003374_003EC0_D43C
4	S1A_IW_GRDH_1SSV_20141121T032002_20141121T032027_003374_003EC0_7916
5	S1A_IW_GRDH_1SSV_20141206T160321_20141206T160346_003600_004413_E5D3
6	S1A_IW_GRDH_1SSV_20141206T160346_20141206T160411_003600_004413_E107
7	S1A_IW_GRDH_1SSV_20141206T160411_20141206T160436_003600_004413_86F6
8	S1A_IW_GRDH_1SDV_20141230T160345_20141230T160410_003950_004C05_486D
9	S1A_IW_GRDH_1SSV_20150108T031950_20150108T032015_004074_004EC5_3794

S1 downloaded product folder name is composed of uppercase alphanumeric characters separated by an underscore (Fig.15). The same naming convention applies for the datasets, but with lower case.

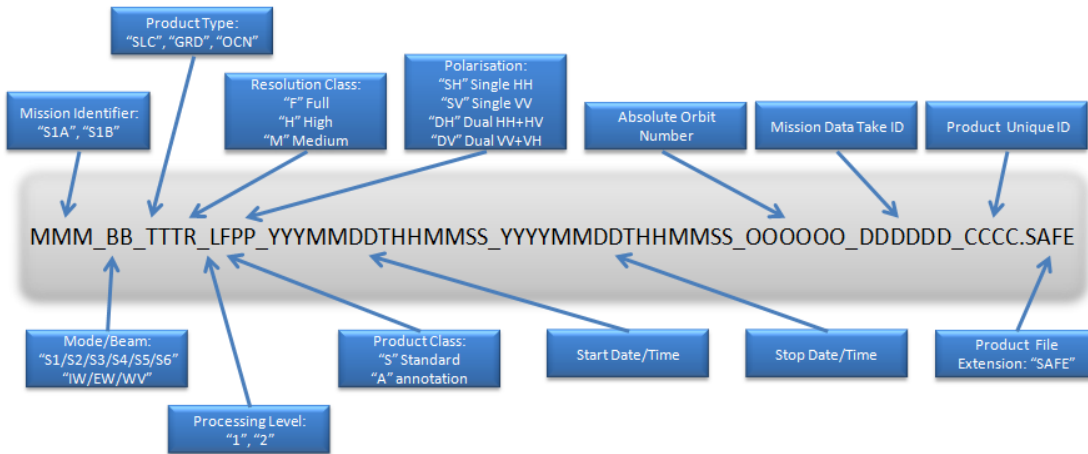


Figure 15: Sentinel-1 product naming convention (Source: ESA, 2014).

The Ground Range Detected High Resolution (GRDH) data is available as “SAFE” extension. Figure 16 show a 10 meter resolution SENTINEL 1 image of 4 October 2014, the image could not be calibrated as calibration coefficient was missing. However the clarity of information was used in visual interpretation and getting more acquainted with the study area.

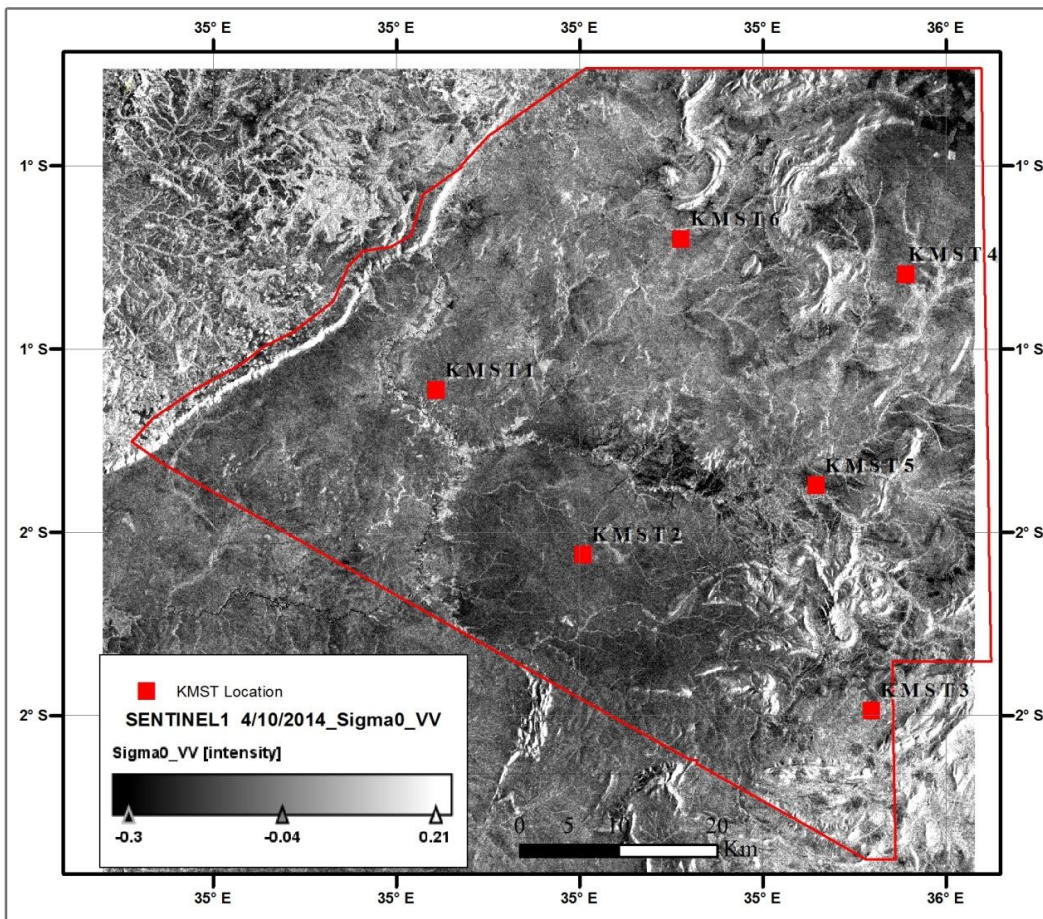


Figure 16: Un-calibrated sentinel-1 SAR intensity image

## 6. SATELLITE DATA PROCESSING

### 6.1. SAR Data

Synthetic Aperture Radar (SAR) processing gives high resolution images from multiple microwave observations. However, this process often leads to speckled images, caused by waves interfering with each other, radiometric accuracy of the sensor as well as distortion of features. It is hard to discern features from speckled images due to degraded quality hence the name “noisy images”. In addition, side looking configuration induces geometric distortions like layover, foreshortening and shadow in mountainous areas. It is therefore important to treat the effects of speckle and geometric distortion in order to obtain accurate geographic information from SAR images.

SAR images were subjected to Range-Doppler ortho-rectification for geocoding of SAR intensity images and 90m SRTM DEM was used for terrain correction and correct for geometric distortions.

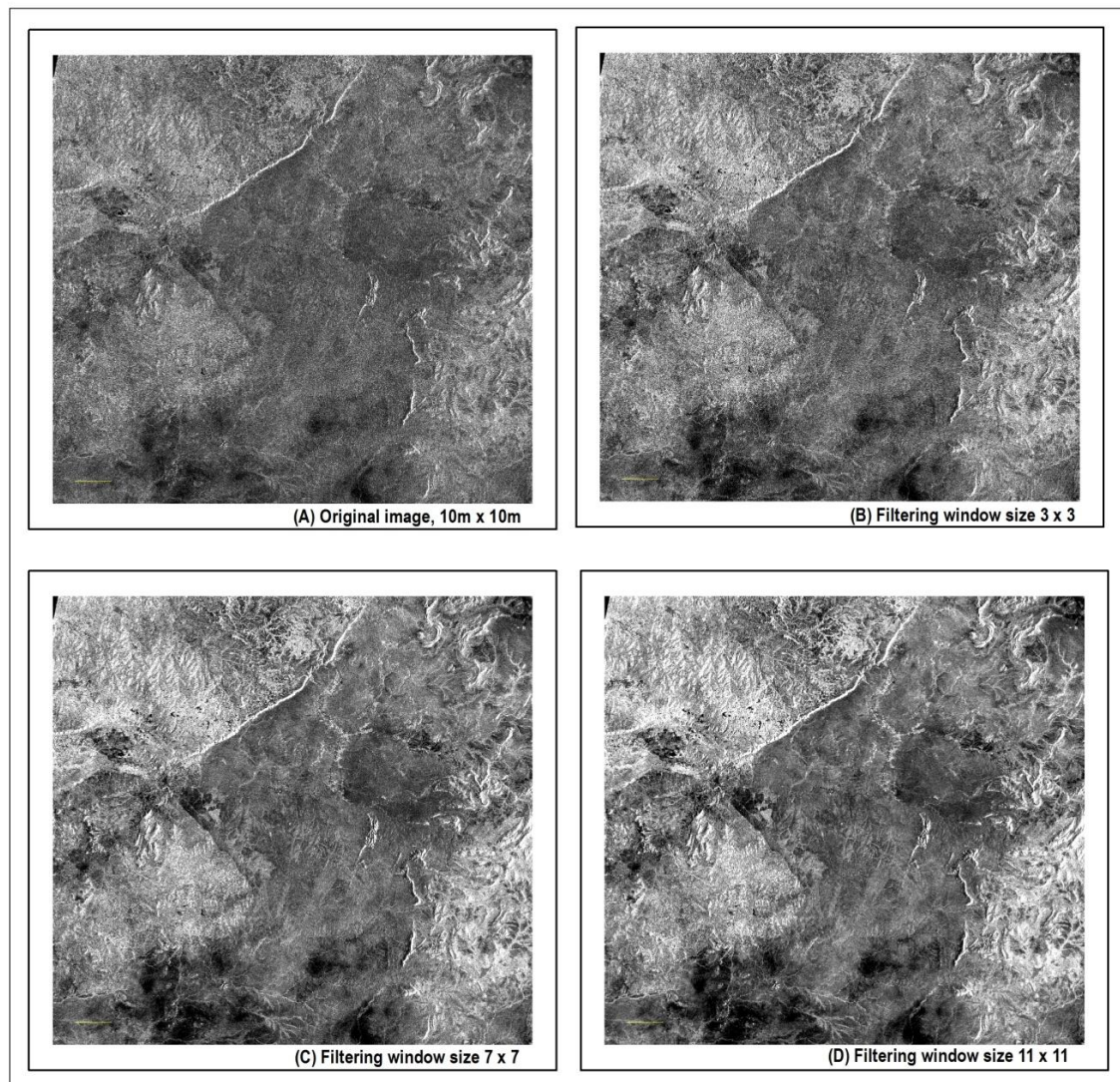


Figure 17: Effect of speckle filtering as a function of filter sizes on interpretability of a SAR image (Sentine-1 image of 4 October 2014).

Radiometric correction was done (only for RADARSAT-2) in order to make SAR pixel values correspond to radar backscatter of the reflecting surface. The SAR backscattering coefficient values were obtained

after pixel aggregation, this was done to match those of MODIS NDVI. The NEST and Sentinel-1 toolbox (S1TBX) by ESA and some scripts were the main processing aid.

Sentine-1 image of 4 October 2014 was subjected to various window sizes (Figure 17) to show the effect of median speckle filtering as a function of filter size on the interpretability of SAR image. The applied speckle filter is based on median of random pixels. Spatial filtering using a moving window was used and the central value in the window or kernel is replaced with the median value. A non-adaptive filtering (Median) was used to reduce the amount of speckle, different kernel sizes of 3x3, 7x7 and 11x11 were chosen. In Figure 17, image (A) show the original image, the effect of speckle is so severe, that interpreting this image is very difficult. A 3x3 filter was applied on image (B), this reduced the amount of speckle but not sufficiently enough to warrant clear interpretation, image (C) show a clear image and easy to interpret, features are easily distinguishable while image (D) more feature have been generalized making the image even more smoother, the image looks sharper, however this larger generalization takes away all the necessary details. Eventually kernel size 7x7 was settled on and applied to SAR datasets.

## **6.2. MODIS NDVI**

The downloaded HDF4 were converted to Tagged Image File Format (TIFF) and reprojected to Geographic coordinate system using MODIS reprojection Tool Kit. The tool was retrieved from USGS Land Processes Distributed Active Archive Centre (LP DAAC) website. The tiles were then mosaicked to cover the study area.

## **6.3. TRMM 3B42v7 rainfall**

The original data format when the images are downloaded is the Network Common Data Format (NetCDF). The files were converted to Tagged Image File Format (TIFF) and then into American Standard Code for Information Interchange (ASCII). The ASCII files were retrieved from the ITC database.

## 7. RESULTS AND DISCUSSION

### 7.1. Kenya Mara Soil Moisture Station

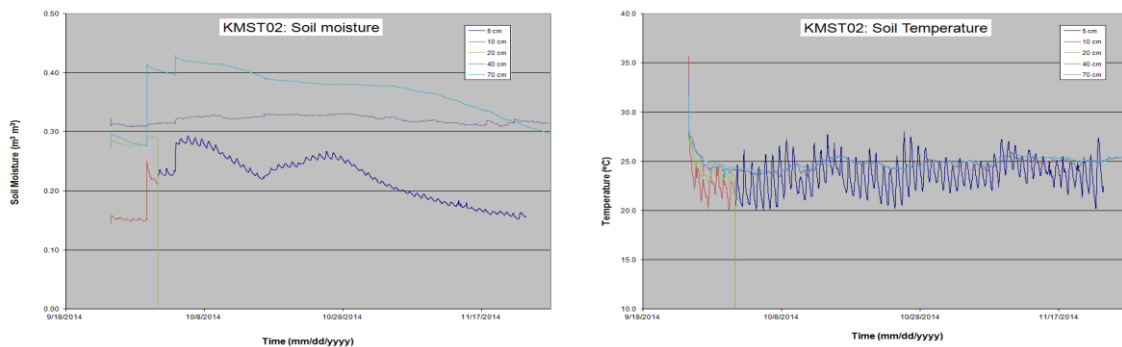
The installation of the soil moisture monitoring stations that can exchange its data via telecommunication networks poses several challenges in a remote area such as the Masai Mara. The connectivity with the nearest telecommunication tower should be sufficient, while also the security of the instrumentation as well as accessibility of the locations need to be taken into consideration. The initial idea was to bury the antenna's connected to the data loggers below the surface under 5 cm of soil and program the logger to transmit its record data twice per day around 12h and 24h local time. In this manner the equipment would not be visible on the surface and the issues with security would be minimized.

Locations were selected where the connectivity with the nearest telecommunication tower would be best. However, it was found that the network connection was unstable, and after installation some of the loggers did not report to the data server for some days. This was rectified by improving on the communication settings. Two measures were taken to increase the likelihood of data being transmitted to the data servers via the telecom network. Firstly, the loggers were reprogrammed to send data four times a day in the morning at 6h, 7h and in the evening at 18h, 19h to avoid interruption due to overload of the network during midday and the shutdown of the network at night. Secondly, the antennas were fully exposed and some were mounted on a wooden pole to maximize its range as is shown in Fig. 18.



Figure 18: Examples of antenna setups improvised to increase the reception with the telecommunication network for the remote exchange of data.

After rectification of the communication settings and exposing the antenna data was relayed to our workstation. Figure 19 shows obtained measurements of soil moisture and temperature of the 6 stations.



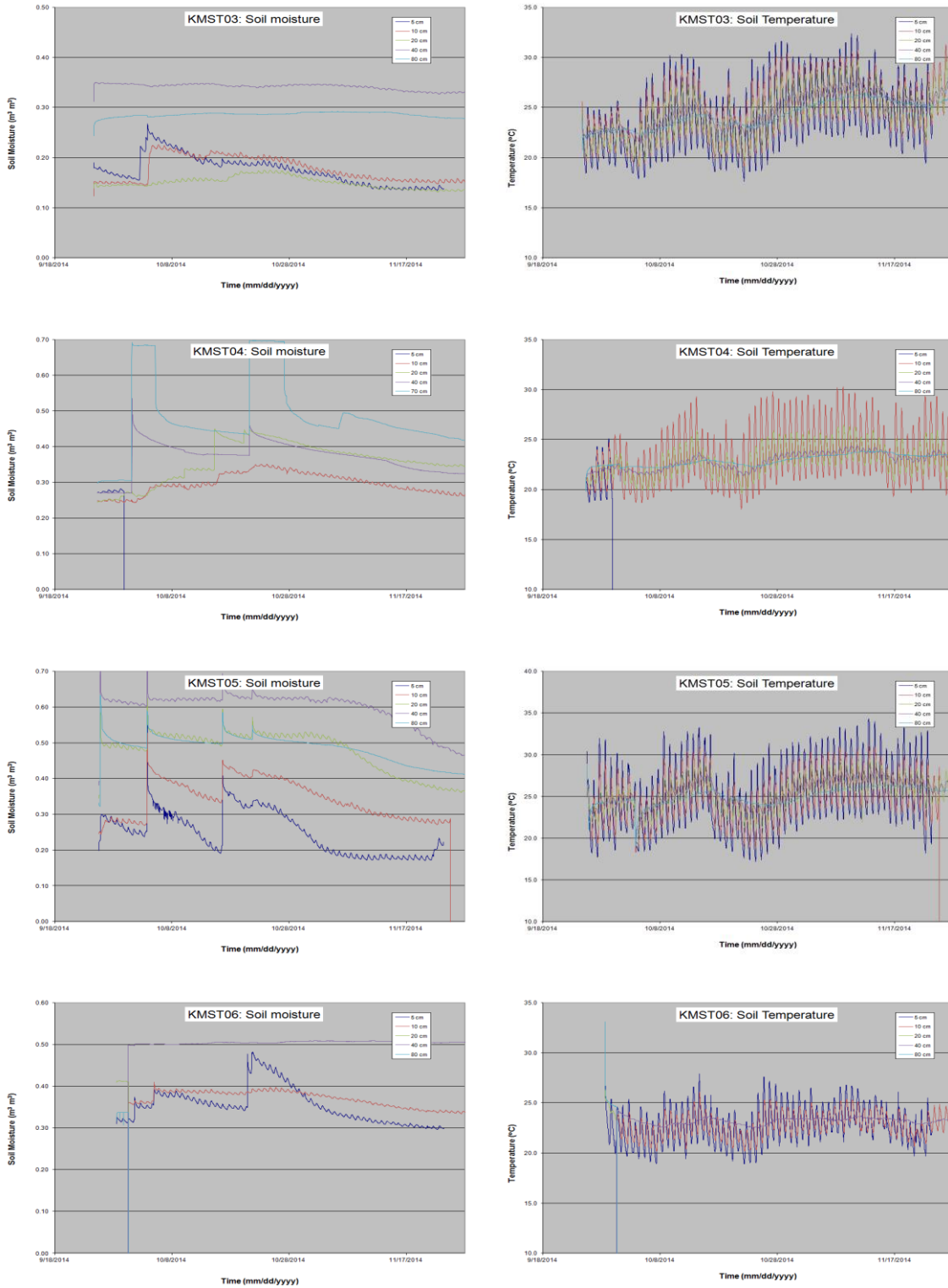


Figure 19: Measured temperature and soil moisture of the KMST in Masai Mara.

Another issue that played an unfortunate role in operating the data loggers was the heavy clay soils (refer to Figure 11 and Table 4). The heavy clay induces severe water logging after rain events. Under such circumstances the data logger is virtually floating in water.

Three measures were taken to prevent water from affecting the data loggers: i) socks filled with silica gel grains were put in the data logger to absorb the water (vapour) that enter the logger's box, ii) the edge of

the data loggers were sealed with silicone kit, and iii) the data loggers were wrapped in multiple layers of plastic and tightly sealed with electric tape. Despite these protection measures the data logger of KMST01 malfunctioned on September 25<sup>th</sup> only two days after installation as seen in Figure 20. Water had entered the data logger and destroyed the electronics. Finally, this was the only station that was destroyed by water.



Figure 20: Inundation land surface conditions destroyed the electronics of the data logger at KMST01 after which communication stopped on September 25<sup>th</sup> 2014.

## 7.2. Temporal backscatter analysis of RADARSAT 2, Rainfall and MODIS NDVI

Season in Mara River Basin (MRB) is divided into two wet seasons. The long rain events occur during the month of April and short rain events fall in the month of September and October. MRB is a region that solely depends on rainfall as source of water for agriculture, then it follows that vegetation growth would also follow the rainfall. Farmers have adapted to planting during the wet season and harvesting during the dry season. Figure 21 shows the daily and cumulative distribution of rainfall over the study period. The cumulative distribution shows the transitions of seasons from wet to dry season.

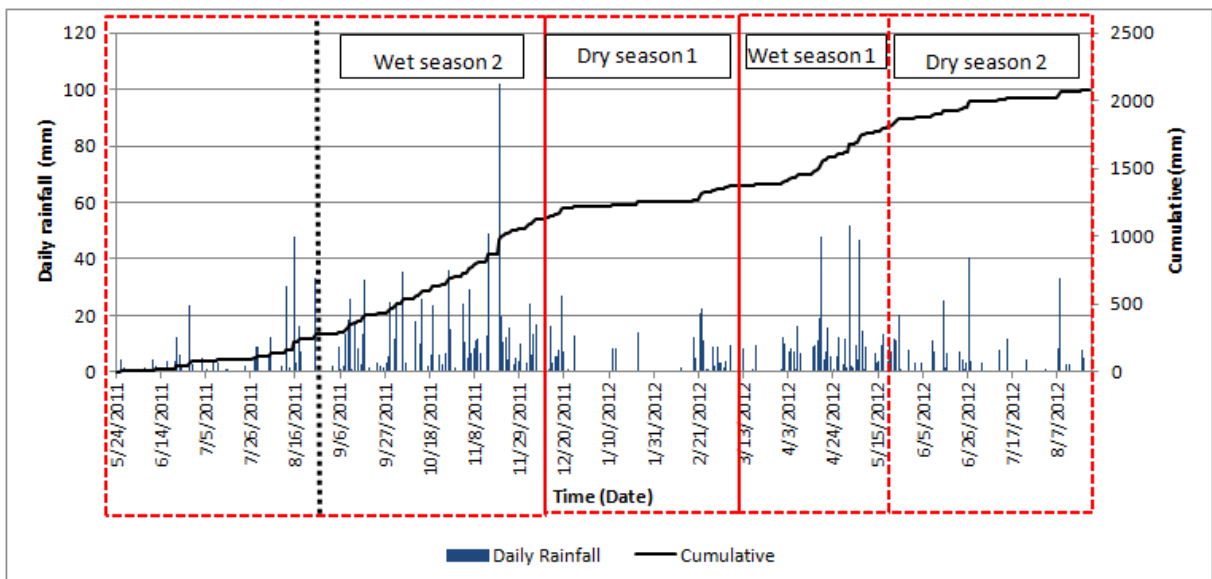


Figure 21: Daily rainfall distribution and seasonal transition of Masai Mara from May 2011 – August 2012

A total of 11 RS2 and MODIS NDVI images of the period between May 2011 and August 2012 were retrieved from the ITC database. The spread of the images made it possible to study temporal variation of

vegetation in relation to RS2 backscatter (dB) and rainfall. It was observed that, during the dry season and the onset of growing period (early wet season) there were small effects of vegetation on SAR backscattering. This trend was seen in both VV and VH polarization. Comparison between MODIS NDVI and RS2 (dB) average values is illustrated in Figure 22. The general trend was that, the SAR backscatter was increasing with the growth of vegetation and decreasing with decrease in vegetation biomass.

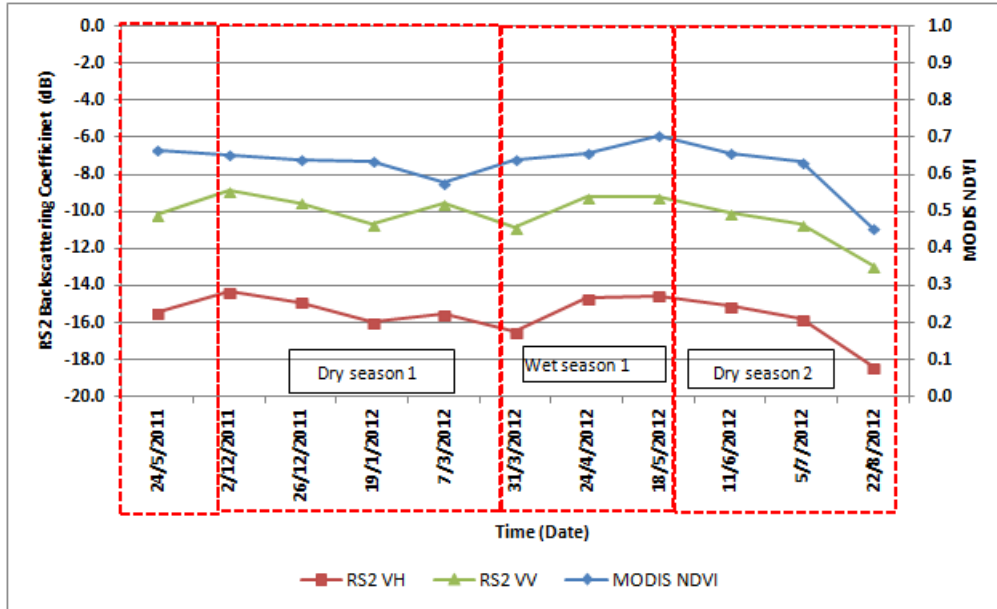


Figure 22: Temporal variation of MODIS NDVI and RS2 Backscatter polarization on the whole study area.

Three areas covered in cropland, savannah grassland and permanent vegetation were selected. For each land cover, RS2 and MODIS NDVI images that correspond to each season were identified and the pixel information retrieved for comparison. The plots in figure 23, 24, 25 and 26 illustrate the impact of the seasonal dynamics in land surface conditions on the temporal variation of the backscattering coefficient of savannah land, cropland, and permanent vegetation. Seasonal comparison was done with the images that fall within that particular season. The boxes show images that correspond to a particular season.

Over the cropland, it was found that, the RS2 had a positive correlation with the MODIS NDVI. The ( $R^2 = 0.59$  VH (dB) and  $0.47$  VV (dB) whole study period (full season) as in Figure 23. It was observed that MODIS NDVI was having a similar trend with VH and VV RS2 backscatter coefficient as illustrated in figure 24.

The  $R^2$  values for each season in Table 10 were obtained from correlation of average values of RS2 and MODIS NDVI of each image. The full season  $R^2$  was obtained from individual pixel comparison as shown in Figure 23,

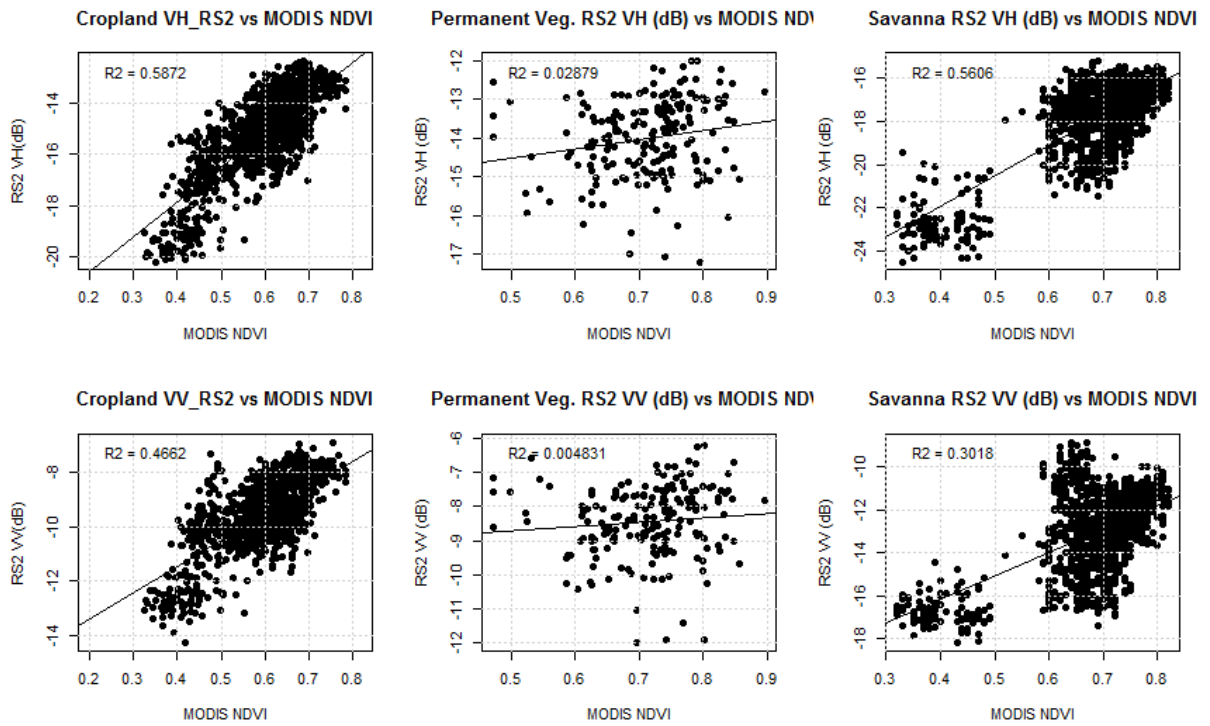


Figure 23: Comparison between RS2 and MODIS NDVI data over cropland, permanent vegetation and savannah land

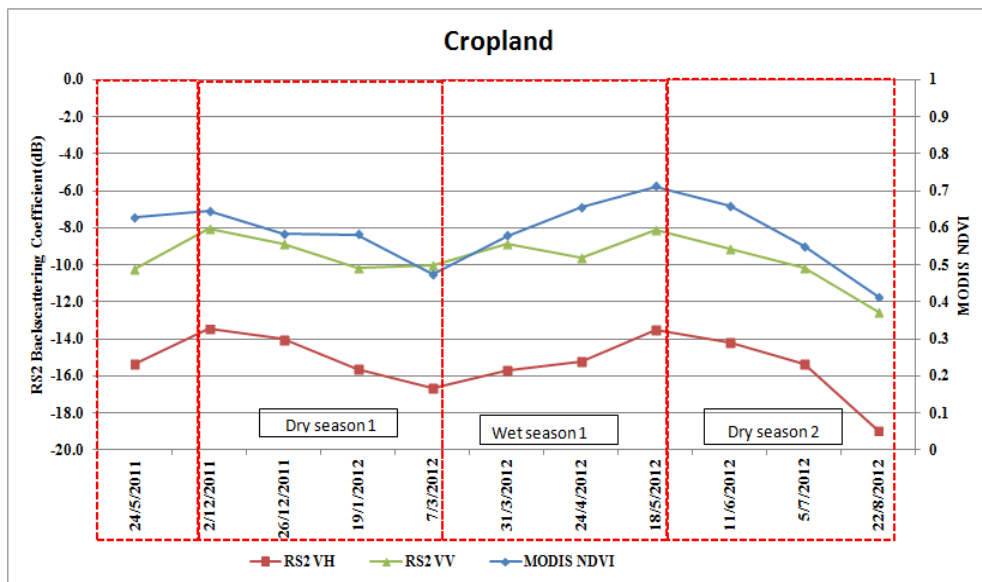


Figure 24: Seasonal variation of MODIS NDVI and RS2 backscattering coefficient over cropland

The  $R^2$  indicate a good correlation between RS2 backscattering coefficient and MODIS NDVI during the dry season1 (Table 10). An upward trend is exhibited during the wet season 1, this is due to the increasing rainfall, which, trigger vegetation growth. This was well represented by an increase of  $R^2$  indicating an increase of biomass as compared to dry season 1.  $R^2 = 0.56$  obtained in VV under farmland was due to its sensitivity to soil moisture and surface roughness. During the dry season 2, the crops have reached their peak and are fully mature, thus giving a very high  $R^2$  of 0.95 for RS2 VH (dB), and RS2 VV (dB) of 0.98, which is the highest. Table 10 shows variation of coefficient of determination over different vegetation types and seasons.

Table 10: Variation of Coefficient of determination ( $R^2$ ) over different vegetation types and seasons

	Coefficient of determination for NDVI and RS2 backscatter					
	Farmland		Permanent Vegetation		Savanna Grassland	
	VH	VV	VH	VV	VH	VV
Dry Season 1	0.81	0.72	0.44	0.25	0.41	0.02
Wet season 1	0.88	0.56	0.02	0.03	0.75	0.55
Dry Season 2	0.95	0.98	0.11	0.09	0.93	0.80
Full Season	0.59	0.47	0.03	0.00	0.56	0.30

In the savannah land or the rangelands a lot of activities take place during certain times of the year, including the famous wildebeest migration in July – November. Millions of wildebeest graze on the grass which has a major impact on the biomass. Figure 25 shows a sharp drop of RS2 backscattering coefficient while MODIS NDVI had a gradual drop in dry season 1. This can be associated with low biomass as a result of the millions of wildebeest grazing on the grass.

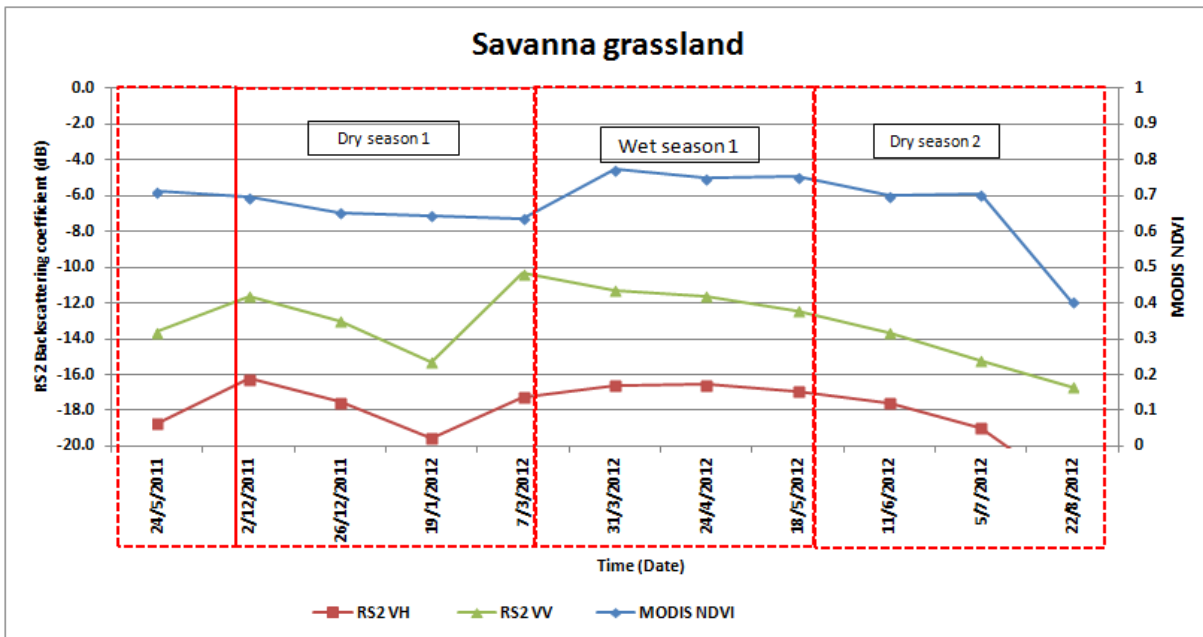


Figure 25: Seasonal variation of MODIS NDVI and RS2 backscattering coefficient over savanna grassland.

At the end of the dry season 1, a sharp increase is seen in VH and gradual increase in VV backscattering coefficient. This is attributed to the soil moisture increase at the onset of the wet season 2. It was also observed that RS2 backscatter coefficient was sensitive to soil moisture. In addition RS2 backscatter coefficient showed a faster response to the growth of vegetation as compared to MODIS NDVI. This can further be evidenced in wet season 2 and dry season 2 in figure 25. In this regard RS2 backscatter coefficient can be used in predicting vegetation availability in Mara savannah. The correlations exhibited by VH polarization can, therefore, be used in estimating dry biomass.

Permanent vegetation does not change much as a result of rainfall variations, since they are not seasonal plants and are very slow to stimuli like rainfall. These are areas covered with bushes or shrubs or forested areas. Figure 26 shows fairly constant backscattering coefficient throughout the season. RS2 backscattering coefficient does not change much due to backscatter from trunks and stems. Coefficient of

determination (refer to table 11) shows low correlation of  $R^2 = 0.44 - 0.11$  for VH polarization and  $R^2 = 0.25 - 0.09$  for VV polarization in dry season 1 and dry season 2 respectively. In the wet season 1 there is very low  $R^2 = 0.02 - 0.03$  for RS2 VH and VV polarizations. This low correlation demonstrate that backscatter over permanent vegetation is determined by branches and trunks and much less by foliage.

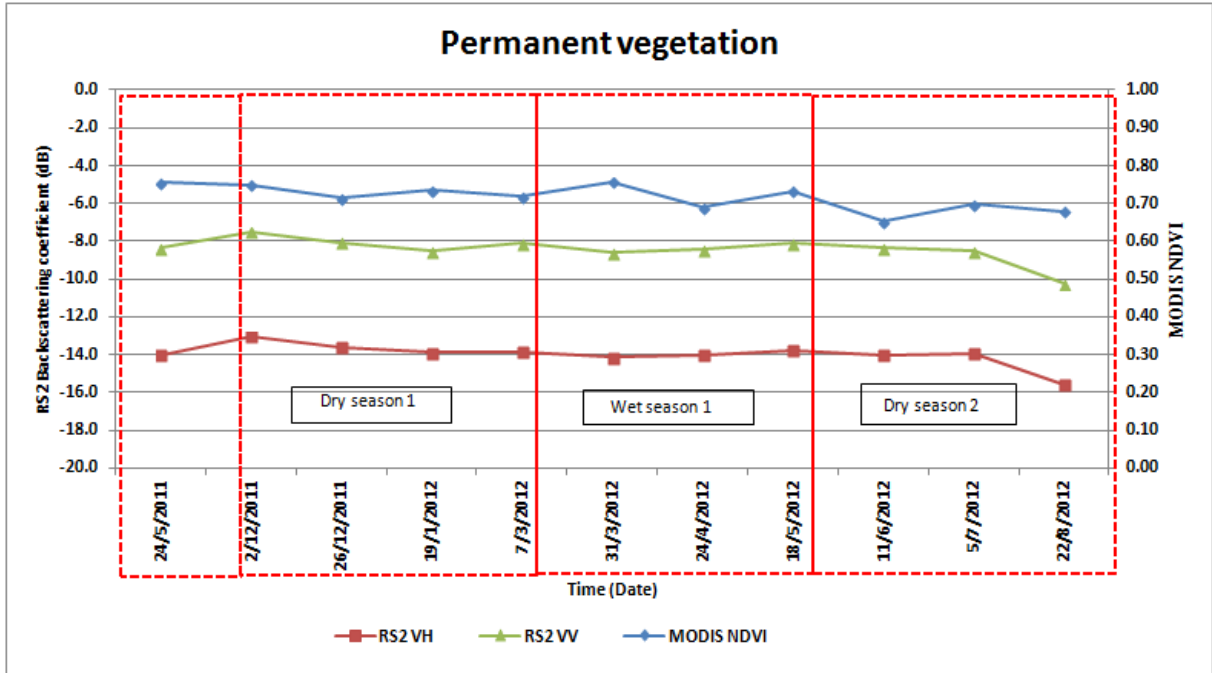


Figure 26: Seasonal variation of MODIS NDVI and RS2 backscattering coefficient over permanent vegetation.

Figure 27 illustrates temporal correlation of MODIS NDVI and RS2 VV (dB). Two stacks were made, one for MODIS NDVI and the other for RS2 each carrying a set of 11 images, the stacks were then correlated. Temporal correlation of SAR backscatter and NDVI showed positive correlation in farmlands, bare and grassland, this was due to the fact that SAR (microwave) is affected by vegetation biomass. It was also observed that there was a negative correlation in regions with permanent vegetation, marshy regions, and waterlogged areas. This was due to saturation of SAR at these regions.

Figure 27 show a Landsat image and the full season correlation. On the Landsat image along the face of the escarpment (permanent vegetation) on it can be seen that there is a negative temporal a correlation of between (-0.51) and (-0.12), this can also be seen on the deep pink region (Marshy) and standing water bodies when compared to the temporal correlation image. These are regions that mostly do not change much with vegetation growth and seasonal variations.

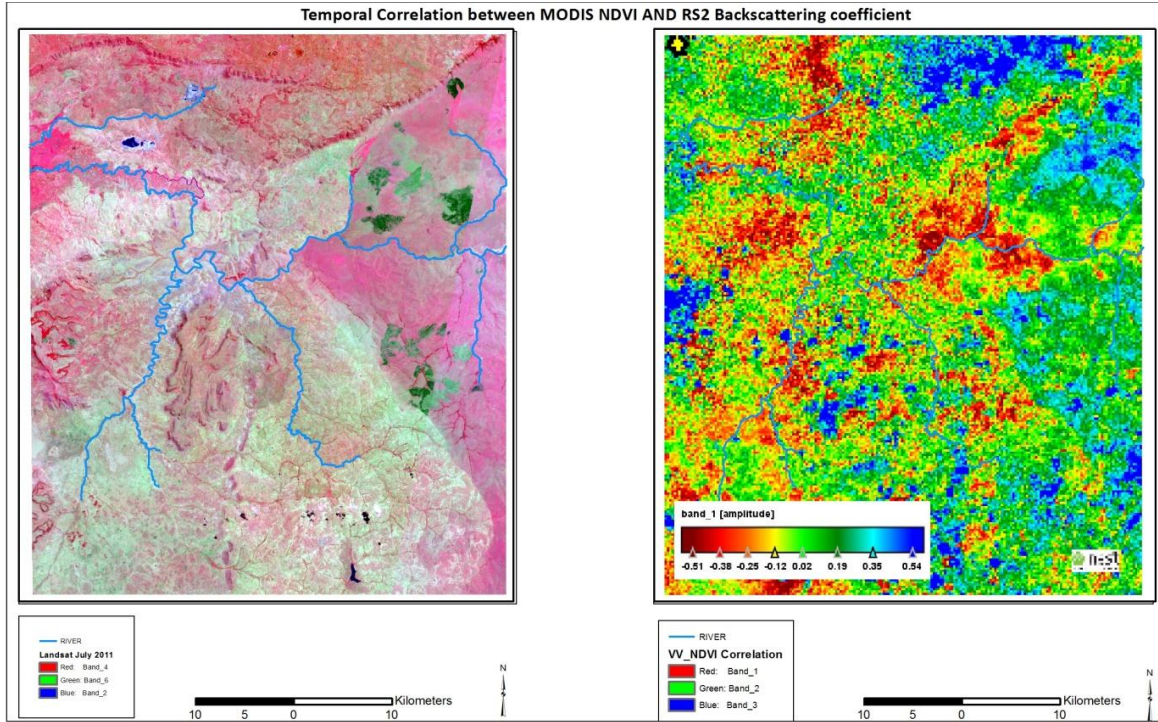


Figure 27: Temporal correlation of MODIS NDVI and RS2 Backscattering coefficient.

### 7.3. RADARSAT-2 depolarization ratio

According to Lin et al., (2009), the merit of using a ratio is that, factors that might affect the absolute backscatter will not impact the relationship with the biophysical variables as long as these factors are affecting VH and VV to the same magnitude. The depolarization or cross - polarization ratio ( $\mathcal{X}_v$ ), is the ratio between VH to VV polarization expressed in dB (Ulaby, Moore, & Fung, 1986; Gherboudj et al., 2011).

$$\mathcal{X}_v = \frac{VH(dB)}{VV(dB)} \quad (4)$$

$$\mathcal{X}_v = VH(dB) - VV(dB) \quad (5)$$

Previous studies have demonstrated that depolarization ratio has the ability to distinguish variations of roughness of bare fields (Ulaby et al., 1986). For studying the effects of the selected land cover types (cropland, savannah, permanent vegetation) on the depolarization ratio, plots of the depolarization ratio with VH (dB) and VV (dB) for each land cover was done, as illustrated in figure 29 and 30.

The data point distribution show a generic rhombus shape, a characteristic associated with depolarization ratio in relation to vegetation and soil moisture (Fig.28). This characteristic is clearly depicted in cropland and savannah grassland, but not for permanent vegetation. It was observed that the depolarization ratio was increasing with increasing VH (dB) hence it can be used in vegetation monitoring.

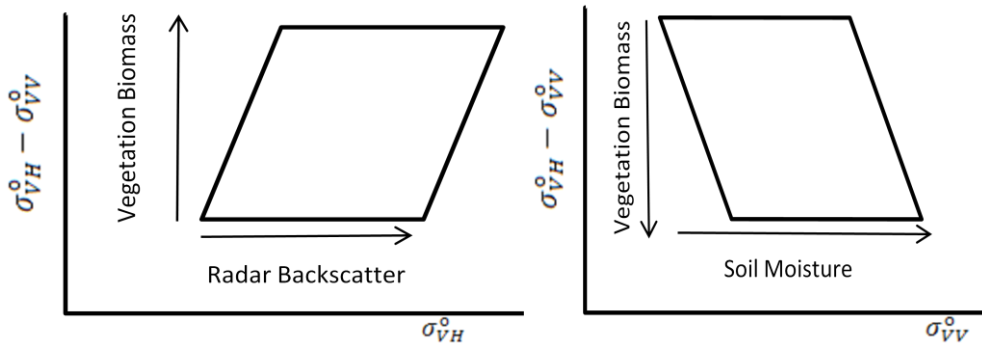


Figure 28: Generic characteristic of depolarization ratio.

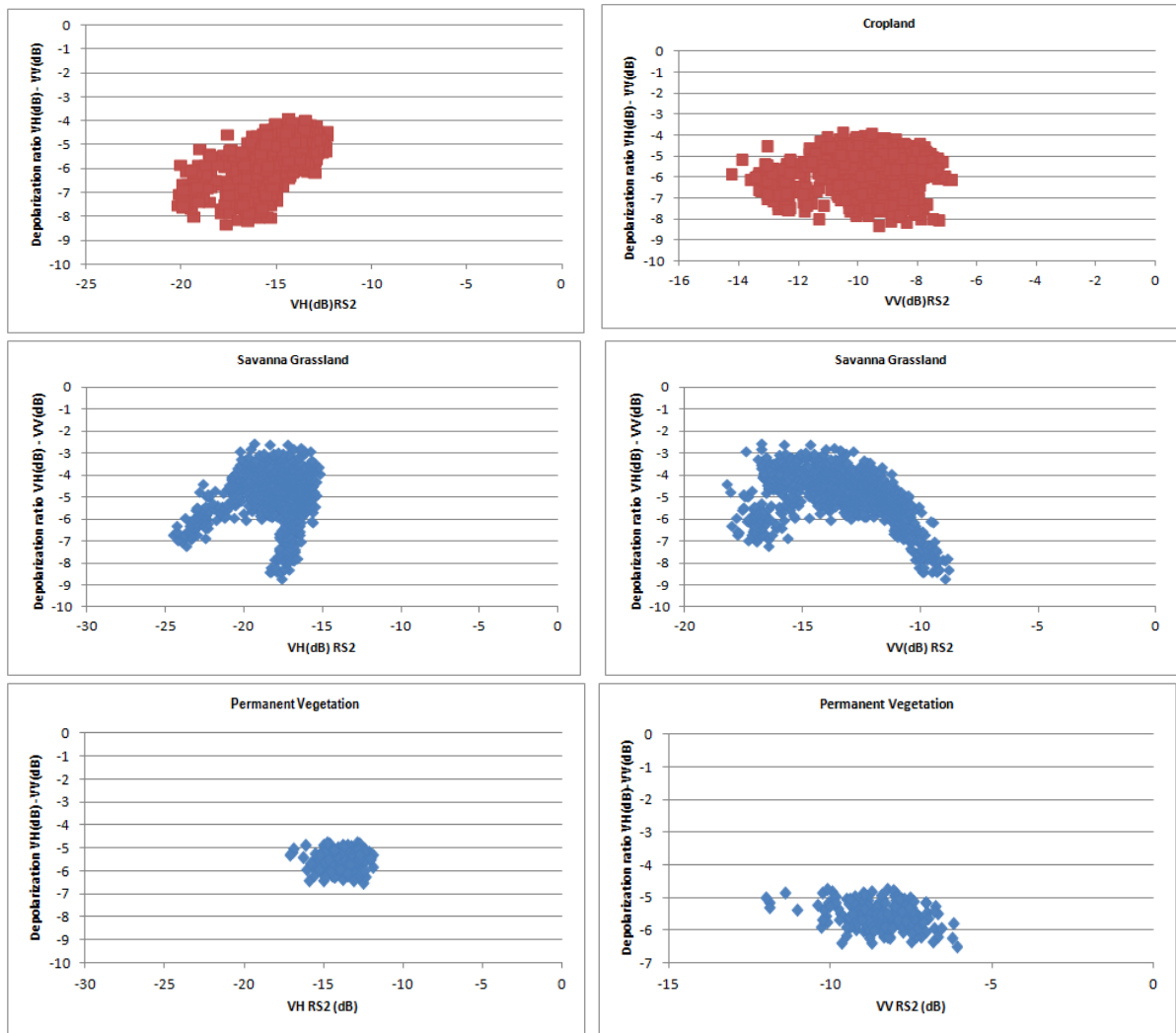


Figure 29: Depolarization ratio of RS2 VH (dB) - VV (dB) showing plots for Cropland, Savannah land and Permanent vegetation.

In this research, the ratio showed a tendency to increase with vegetation growth i.e. MODIS NDVI (Fig.29), this was attributed to the increasing tendency of both VH(dB) and VV(dB) to vegetation growth as earlier demonstrated in section 7.2. In relation to VV, it was observed that, as the depolarization ratio decreases (vegetation biomass) VV was increasing (sensitivity to soil moisture). The temporal correlation of MODIS NDVI and RS2 SAR ratio data showed an improvement in coefficient of determination in favour of both polarizations as in Table 11.

Table 11: Variation of Coefficient of determination ( $R^2$ ) over different vegetation types and seasons as a function of depolarization ratio (average pixel values)

Coefficient of determination for MODIS NDVI and RS2 VH (dB) -VV (dB)			
	Farmland	Permanent Vegetation	Savannah Grassland
	VH (dB) –VV(dB)	VH(dB) – VV (dB)	VH (dB) – VV (dB)
Dry Season 1	0.77	0.05	0.23
Wet Season 1	0.72	0.04	0.79
Dry Season 2	0.65	0.003	0.79
Full Season	0.38	0.0	0.14

Figure 30 illustrates the trend in depolarization ratio and MODIS NDVI over cropland, savannah and permanent vegetation. Figure (a), show a clear pattern of increase of the ratio to biomass increase, which is the same trend to figure (b), however there is minimal almost non response to permanent vegetation, which cements the fact that backscatter from permanent vegetation is from trunk and branches, and less from foliage.

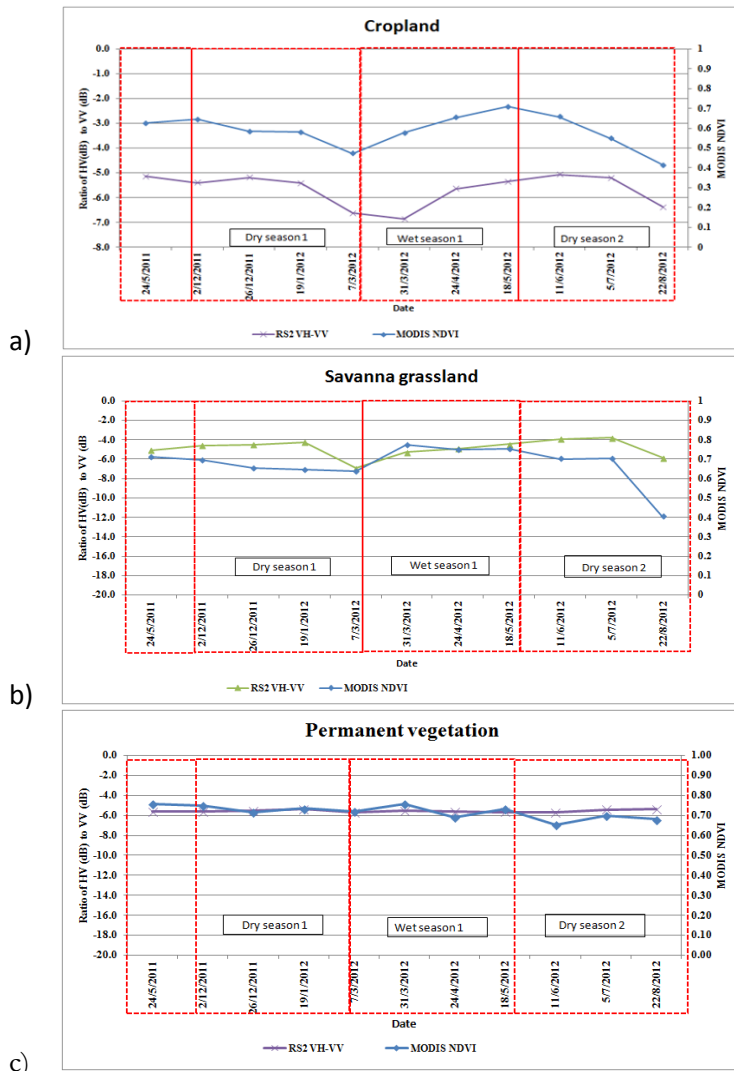


Figure 30: Variation of the ratio VH (dB) to VV (dB) plotted against MODIS NDVI over selected land cover a) cropland b) Savanna grassland c) Permanent vegetation.

The depolarization ratio draws its strength from the shortcomings of the individual dual SAR data. The improved coefficient of determination could be because of different backscattering mechanism of VV (dB) and VH (dB).

#### 7.4. Spatial backscatter variability and standardized anomaly

The variation of dielectric properties (soil, vegetation) and geometry of land have effect on radar backscatter signal. Land surface can be bare, or covered by grass, shrubs, dense vegetation, and even by open water. These regions are expected to have different response to radar signal since their dielectric and geometry properties are different.

To identify the spatial variability of RS2 backscatter, RGB composite of the dual RS2 was made for each image to aid in visual interpretation. Figure 31 shows image of dry (19 Jan 2012) and wet (18 May 2012) seasons. It was found that the greenish colour represents the presence of vegetation, these are regions that  $VH (dB) > VV (dB)$ . The purple regions are associated with bare areas, in these regions  $VV (dB) > VH (dB)$ . The black and smooth areas represent low backscatter associated with specular reflection (Mostly open water) both in VV (dB) and VH (dB). It was also noticed that regions with dense permanent vegetation were showing stable backscatter response both in the wet and the dry seasons, in agreement with (Mtamba, van der Velde, Ndomba, Zoltán, & Mtalo, 2015), as can be seen in both images (White areas).

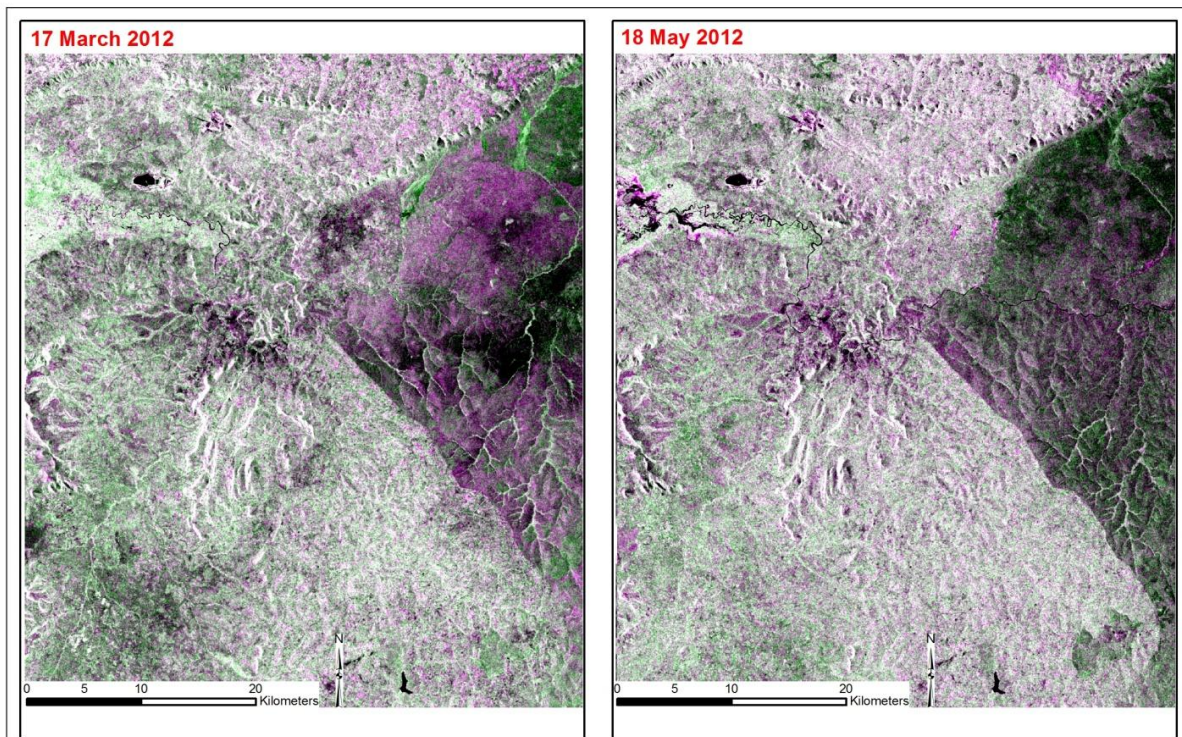


Figure 31: RGB composite of 2 RS2 SAR for dry (19 Jan 2012) and wet (18 May 2012) season. The composites were made of R (VV), G (VH), and B (VV).

In order to understand the effect of spatial variability on the radar backscatter, evaluation of anomalies was done. An anomaly is an event that does not conform to the normal pattern of a situation at a certain time. It could be a point in a series of data, or failure of a sensor on Earth observation satellite. Statistical anomaly is obtained by subtracting mean values from individual events, then dividing by the standard deviation. In this study Equation 6 was used in detecting soil moisture anomaly.

$$N = \frac{\sigma^0 - \overline{\sigma^0}}{STD(\sigma^0)} \quad (6)$$

Where N is the standardized anomaly,  $\sigma^0$  is the backscatter coefficient,  $\overline{\sigma^0}$  is the mean of  $\sigma^0$  and STD ( $\sigma^0$ ) stands for the standard deviation.

A stack of the 11 RS2 SAR images was made and then, mean and standard deviation were computed for both the VV (dB) and VH (dB) polarizations. Figure 32 shows the maps of the mean and standard deviation backscatter values of RS2 VV (dB) polarization images. The darker smooth tones on the mean backscatter image shows high STD backscatter values, the low mean backscatter can be attributed to specular reflection associated with open water, while the high STD is due to wind and waves on the water surface. The dark rough shades (mean map) are regions occasionally covered in water and vegetation, but the vegetation is short enough to expose water, thus mixed pixels and high STD backscatter values. The shades of brighter regions (refer to mean map) are areas covered in bushy vegetation thus high backscatter as a result of double bouncing of the backscatter. However these regions are showing low STD values because of minimal change in trunk and branches, which are the main backscatter agents.

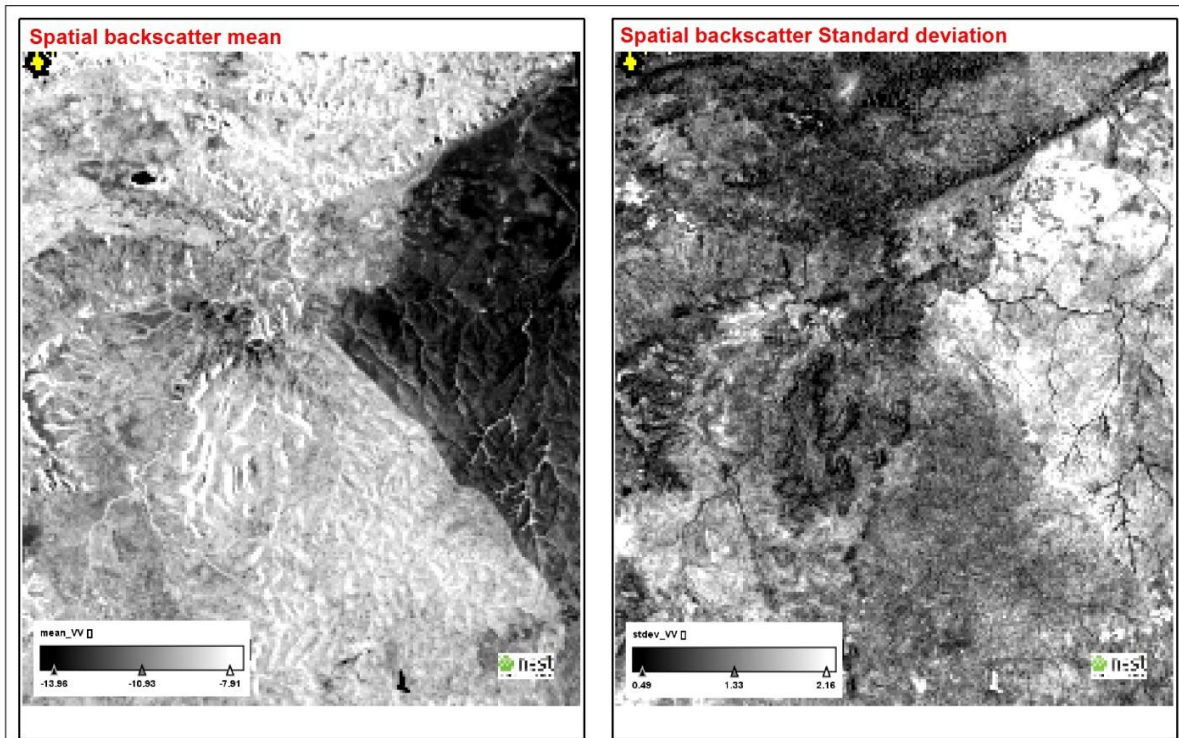
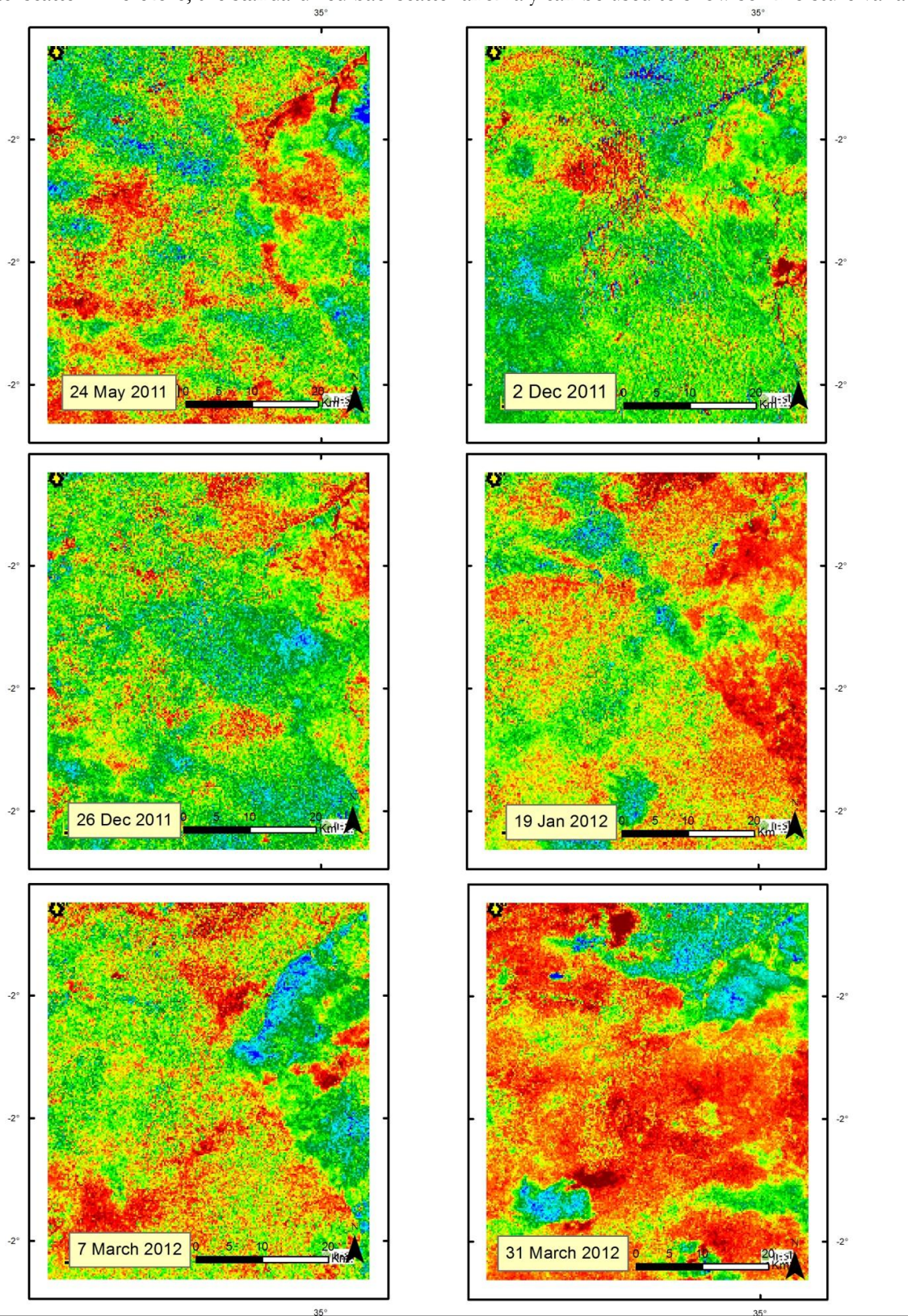


Figure 32: Mean and standard deviation of RADARSAT 2 VV polarization.

Using Equation 6, standardized anomaly was computed for each of the RS2 VV (dB) data. It was observed that, the spatial backscatter variability increases with rainfall availability i.e. during the wet season, this variation increases due to spatial differences in soil thermal and hydraulic properties. The low backscatter variability in this case was associated with homogenous spread of rainfall, and spatial variability nature of rainfall. It was also observed that, the presence of vegetation was influencing the variation. Figure 33 shows spatial-temporal variation of backscatter caused by the land dynamics and rainfall availability. It can be seen that regions with low mean and high standard deviation are showing higher probabilities of water cover (inundation). Notable inundation can be found on the 18 May 2012, this is a period after long rain event.

The standardized backscatter anomaly was increasing with presence of soil moisture. However, where there is inundation, the anomaly tended to decrease. This was associated with saturation of radar backscatter. Therefore, the standardized backscatter anomaly can be used to show soil moisture variation.



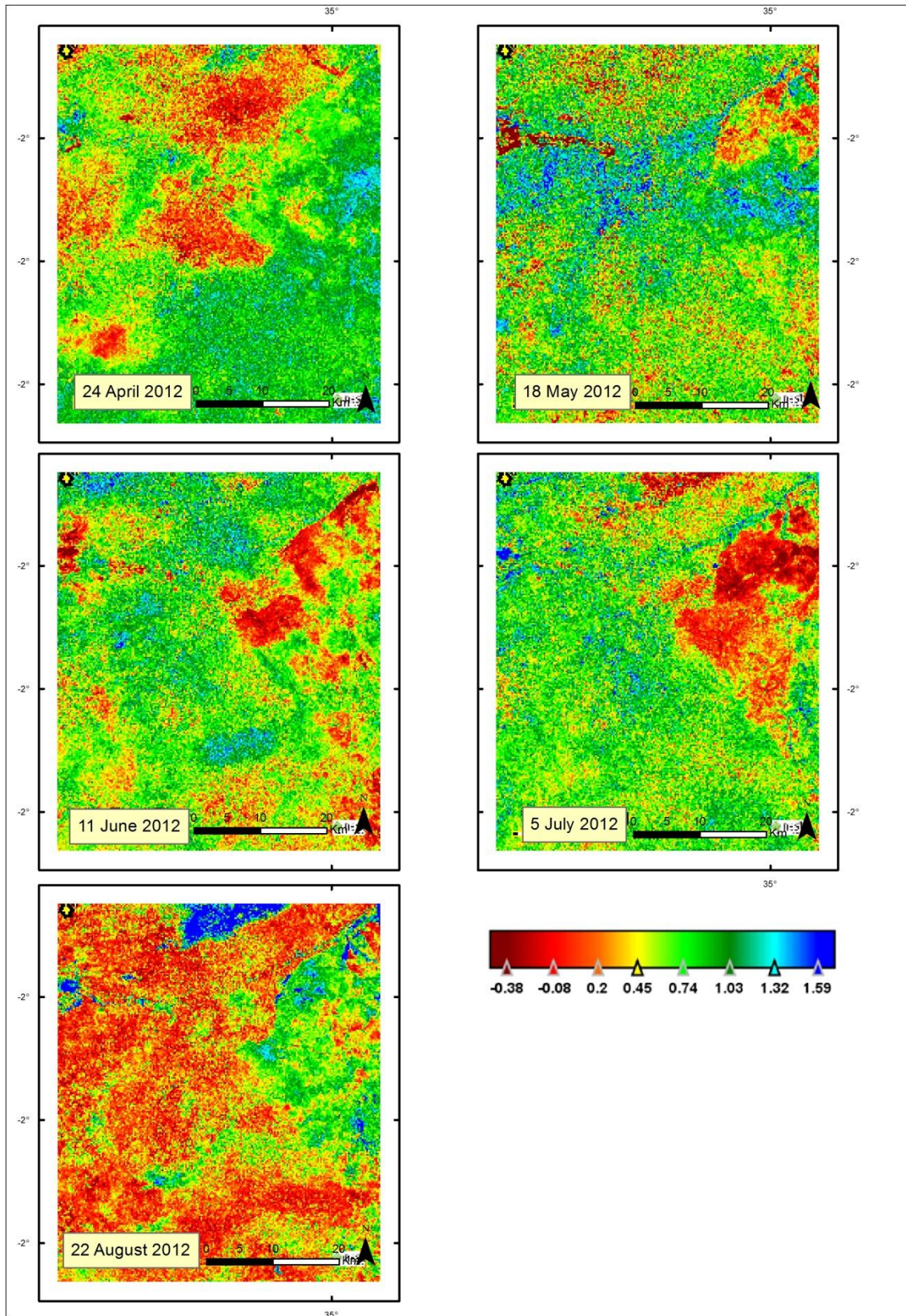


Figure 33: Spatial backscatter variability as a function of mean and standard deviation.

### 7.5. Sentinel-1 Analysis

Although Sentinel-1 data was un-calibrated, it was used in qualitative assessment of backscatter anomaly. Processing procedure adopted in determining standard anomaly in RADARSAT-2 was applied for Sentinel-1 using the eight images. Figure illustrates backscatter anomaly of sentinel-1.

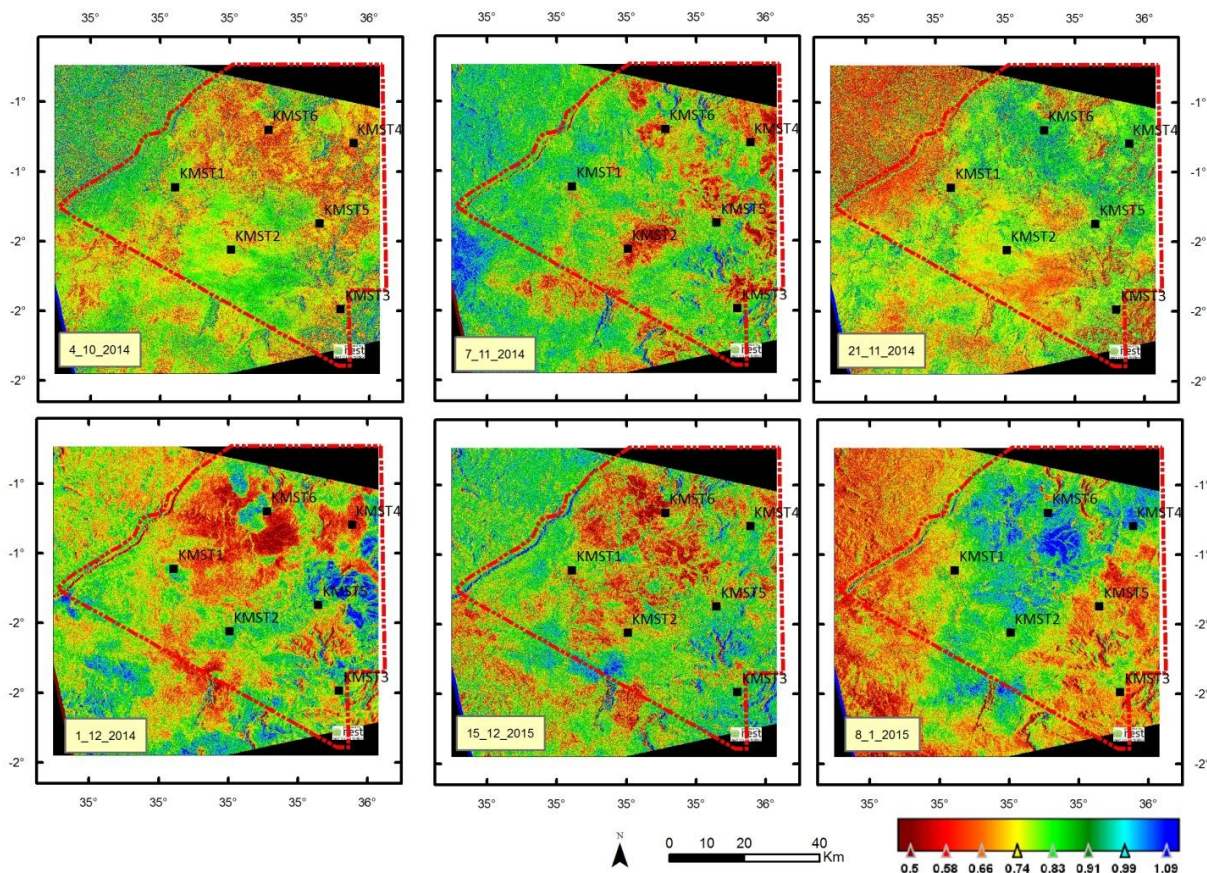
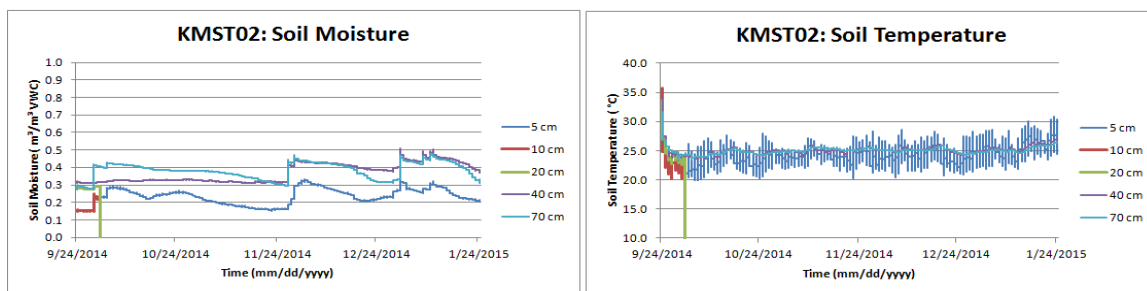


Figure 34: Standardized backscatter anomaly of (Un-calibrated) Sentinel-1

The short rain events occur during November – December months. From visual inspection of the sentinel-1 maps, and KMST soil moisture measurements (Fig.35), a similarity was observed for each station to correspond to KMST measurements. The maps are showing a transition towards the dry season that occurs between January and March i.e. at each image the spread of low values is increasing, indicating the spread of onset of the dry season.



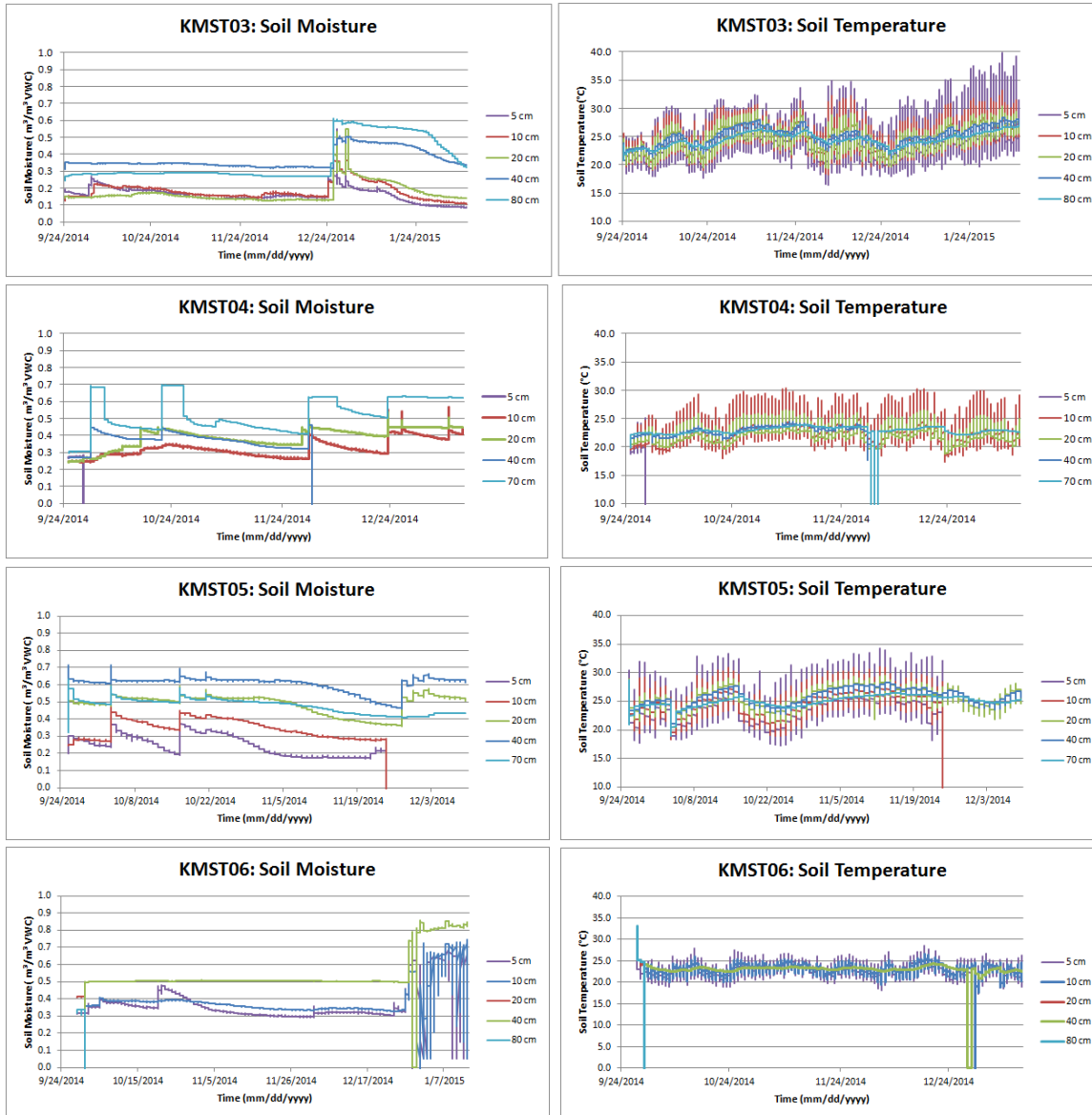


Figure 35: KMST measurements of soil moisture and soil temperature.

### 7.6. Comparison between Sentinel-1 and RADARSAT-2

Backscatter anomaly maps of Sentinel-1 and RADARSAT-2 that correspond to each other were selected. The selected dates fall within the same season and month. Visual interpretation by marching the two maps showed similar pattern. Figure 36 is showing the dates selected for comparison.

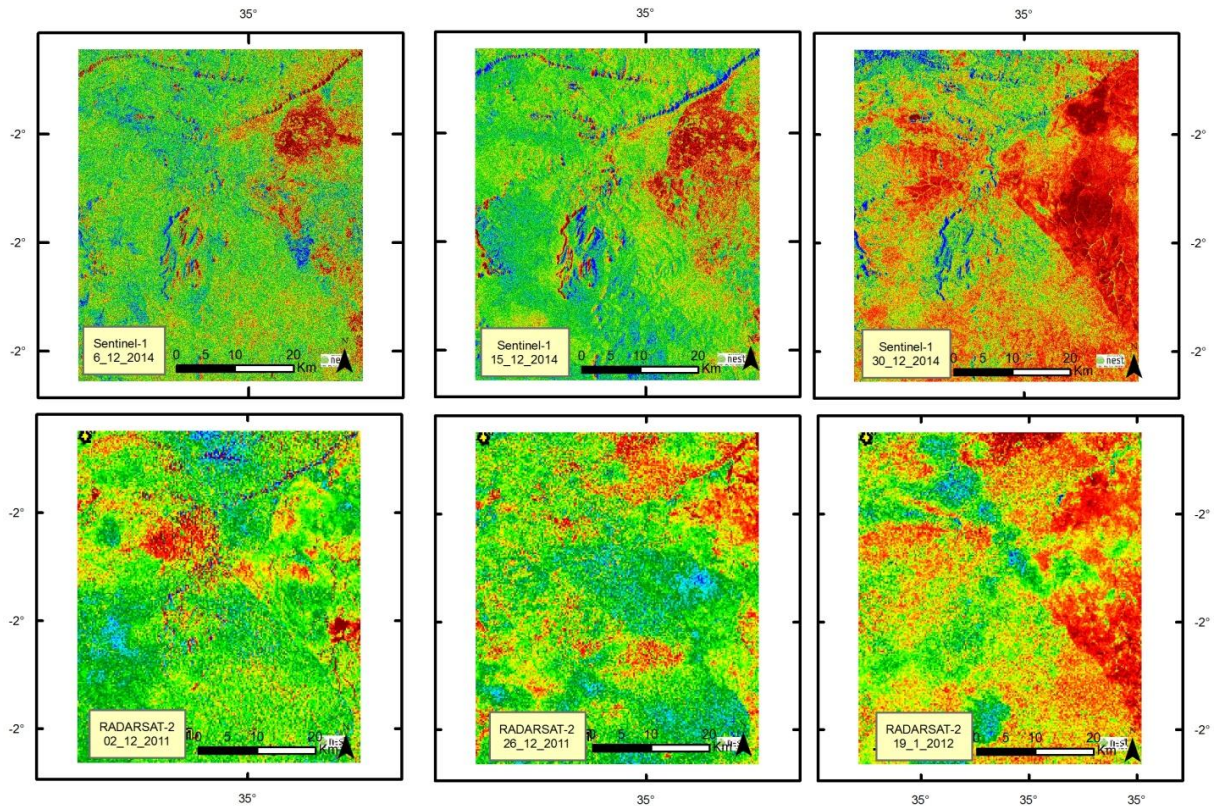


Figure 36: Comparison between Sentinel-1 and RADARSAT 2

In both maps it can be seen that the low soil moisture values are spreading as the season is changing towards the dry season. This transition is in agreement with the seasonal rainfall events i.e. during the dry months of January and December.

## 8. CONCLUSION AND RECOMMENDATIONS

### 8.1. Conclusion

The main objective of this research was to evaluate the effects of vegetation on SAR backscatter using dual polarized RADARSAT-2 SAR C-band towards processing of sentinel-1 for soil moisture retrieval.

Temporal and spatial variation of the backscattering coefficient of RS2 VV and VH as a function of MODIS NDVI and rainfall was done; the results showed increasing backscattering trend of RS2 data with vegetation growth. The standardized backscatter and the anomaly maps were used to show soil moisture variability.

- Different vegetation types have different magnitudes of effect on SAR backscatter. Cropland and savanna showed greater correlation than permanent vegetation. The cross-polarized backscatter VH showed high correlation with MODIS NDVI, therefore it can be used for vegetation monitoring. The co-polarized backscatter VV can be used in soil moisture monitoring.
- Depolarization ratio ( $X_v$ ) showed a good relationship with MODIS NDVI, therefore it can also be used in vegetation monitoring.
- The field measurements of soil moisture from the near real time monitoring network showed a similar pattern with un-calibrated Sentinel-1. Spatial variability of soil moisture illustrated by the anomaly maps was in agreement with the in-situ soil moisture measurements.
- The anomaly maps showed variation of soil moisture in addition, they also showed regions that are inundated after the long rain events of April-May. Therefore SAR data can also be used for demarcating the flood extent.

### 8.2. Recommendations

From the findings in this study, the following can be recommended:

- To understand the full potential of Sentinel-1 data, there is need to fully calibrate the data, this would enable quantitative analysis.
- A better understanding is required on the effects of natural vegetation on radar backscatter. This because different vegetation types have different effects on radar backscatter.
- More effort should be put in understanding the dual polarized data and how it can be used to correct for the vegetation effect in soil moisture studies.
- Replacing the destroyed KMST01 and possibly adding more would be important in capturing local soil moisture variation, as this would improve on the SAR soil moisture validation.

## LIST OF REFERENCES

---

- Bhola, N., Ogotu, J. O., Said, M. Y., Piepho, H.-P., & Olf, H. (2012). The distribution of large herbivore hotspots in relation to environmental and anthropogenic correlates in the Mara region of Kenya. *The Journal of Animal Ecology*, 81(6), 1268–87. doi:10.1111/j.1365-2656.2012.02000.x
- Bindlish, R., & Barros, A. P. (2000). Multifrequency Soil Moisture Inversion from SAR Measurements with the Use of IEM. In *Remote Sensing of Environment* (Vol. 71, pp. 67–88).
- Bond, M. (2003). *Principles of Wildlife Corridor Design*. Retrieved from <http://www.biologicaldiversity.org/publications/papers/wild-corridors.pdf>
- Brutsaert, W. (2005). *Hydrology: An Introduction*. Cambridge University Press.
- Dessu, S. B., Melesse, A. M., Bhat, M. G., & McClain, M. E. (2014). Assessment of water resources availability and demand in the Mara River Basin. *CATENA*, 115, 104–114. doi:10.1016/j.catena.2013.11.017
- Dubois, P. C., van Zyl, J., & Engman, T. (1995). Measuring soil moisture with imaging radars. *IEEE Transactions on Geoscience and Remote Sensing*, 33(4), 915–926. doi:10.1109/36.406677
- Engman, E. T., & Chauhan, N. (1995). Status of microwave soil moisture measurements with remote sensing. *Remote Sensing of Environment*, 51(1), 189–198.
- Eoportal. (2014). RADARSAT-2 - eoPortal Directory - Satellite Missions. Retrieved December 09, 2014, from <https://directory.eoportal.org/web/eoportal/satellite-missions/r/radarsat-2>
- ESA. (2014). European Space Agency. Retrieved June 02, 2014, from [http://www.esa.int/Our\\_Activities/Observing\\_the\\_Earth/Copernicus/Sentinel-1](http://www.esa.int/Our_Activities/Observing_the_Earth/Copernicus/Sentinel-1)
- FDC. (1989). Copernicus in brief. Retrieved February 01, 2015, from <http://www.copernicus.eu/pages-principales/overview/copernicus-in-brief/>
- Fung, A., & Eom, H. (1985). A Comparison between Active and Passive Sensing of Soil Moisture from Vegetated Terrains. *IEEE Transactions on Geoscience and Remote Sensing*, GE-23(5), 768–775. doi:10.1109/TGRS.1985.289396
- Gherboudj, I., Magagi, R., Berg, A. A., & Toth, B. (2011). Soil moisture retrieval over agricultural fields from multi-polarized and multi-angular RADARSAT-2 SAR data. *Remote Sensing of Environment*, 115(1), 33–43. doi:10.1016/j.rse.2010.07.011
- Kornelsen, K. C., & Coulibaly, P. (2013). Advances in soil moisture retrieval from synthetic aperture radar and hydrological applications. *Journal of Hydrology*, 476, 460–489. doi:10.1016/j.jhydrol.2012.10.044
- Lamprey, R. H., & Reid, R. S. (2004). Expansion of human settlement in Kenya's Maasai Mara: what future for pastoralism and wildlife? *Journal of Biogeography*, 31(6), 997–1032. doi:10.1111/j.1365-2699.2004.01062.x
- Lillesand, T., Kiefer, R. W., & Chipman, J. (2008). *Remote Sensing and Image Interpretation* (6th ed.). John Wiley and Sons.
- Lin, H., Chen, J., Pei, Z., Zhang, S., & Hu, X. (2009). Monitoring Sugarcane Growth Using ENVISAT ASAR Data, 47(8), 2572–2580.

- Mango, L. M., Melesse, A. M., McClain, M. E., Gann, D., & Setegn, S. G. (2011). Land use and climate change impacts on the hydrology of the upper Mara River Basin, Kenya: results of a modeling study to support better resource management. *Hydrology and Earth System Sciences*, 15, 2245–2258.
- Mati, B. M., Mutie, S., Gadain, H., Home, P., & Mtalo, F. (2008). Impacts of land-use/cover changes on the hydrology of the transboundary Mara River, Kenya/Tanzania. *Lakes & Reservoirs: Research & Management*, 13(2), 169–177. doi:10.1111/j.1440-1770.2008.00367.x
- Mtamba, J., van der Velde, R., Ndomba, P., Zoltán, V., & Mtalo, F. (2015). Use of Radarsat-2 and Landsat TM Images for Spatial Parameterization of Manning's Roughness Coefficient in Hydraulic Modeling. *Remote Sensing*, 7(1), 836–864. doi:10.3390/rs70100836
- NASA. (2014a). NASA Aquarius Mission. Retrieved August 17, 2014, from <http://aquarius.nasa.gov/>
- NASA. (2014b). TRMM. Retrieved December 11, 2014, from <http://trmm.gsfc.nasa.gov/>
- Njoku, E. G., & Kong, J.-A. (1977). Theory for passive microwave remote sensing of near-surface soil moisture. *Journal of Geophysical Research*, 82(20), 3108–3118. doi:10.1029/JB082i020p03108
- Ogotu, J. O., Owen-Smith, N., Piepho, H.-P., & Said, M. Y. (2011). Continuing wildlife population declines and range contraction in the Mara region of Kenya during 1977-2009. *Journal of Zoology*, 285(2), 99–109. doi:10.1111/j.1469-7998.2011.00818.x
- Ottichilo, W. K., Leeuw, J. De, Skidmore, A. K., Herbert, H., Prins, T., & Said, M. Y. (2000). Population trends of large non-migratory wild herbivores and livestock in the Masai Mara, 202–216.
- Paloscia, S., Pettinato, S., Santi, E., Notarnicola, C., Pasolli, L., & Reppucci, A. (2013). Soil moisture mapping using Sentinel-1 images: Algorithm and preliminary validation. *Remote Sensing of Environment*, 134, 234–248. doi:10.1016/j.rse.2013.02.027
- Patel, N. R., Anapashsha, R., Kumar, S., Sah, S. K., & Dadhwal, V. K. (2009). Assessing potential of MODIS derived temperature/vegetation condition index (TVDI) to infer soil moisture status. *International Journal of Remote Sensing*, 30(1), 23–39.
- Petropoulos, G. P. (2014). *Remote Sensing of Energy Fluxes and Soil Moisture Content*. Taylor and Francis Group. Retrieved from [http://en.wikipedia.org/wiki/Artisanal\\_mining](http://en.wikipedia.org/wiki/Artisanal_mining)
- Rahimzadeh-Bajgiran, P., Berg, A. A., Champagne, C., & Omasa, K. (2013). Estimation of soil moisture using optical/thermal infrared remote sensing in the Canadian Prairies. *ISPRS Journal of Photogrammetry and Remote Sensing*, 83, 94–103. doi:10.1016/j.isprsjprs.2013.06.004
- Sandells, M. J., Davenport, I. J., & Gurney, R. J. (2008). Passive L-band microwave soil moisture retrieval error arising from topography in otherwise uniform scenes. *Advances in Water Resources*, 31(11), 1433–1443.
- Seneviratne, S. I., Corti, T., Davin, E. L., Hirschi, M., Jaege, E. B., Lehner, I., ... Teuling, A. J. (2010). Investigating soil moisture–climate interactions in a changing climate: A review - Investigating soil moisture–climate interactions in a changing climate A review.pdf. *Earth-Science Reviews*, 99, 125–161.
- Su, Z. (2002). The Surface Energy Balance System (SEBS) for estimation of turbulent heat fluxes. *Hydrology and Earth System Sciences*, 6(1), 85–99. Retrieved from <http://www.hydrol-earth-syst-sci.net/6/85/2002/hess-6-85-2002.pdf>

- Su, Z. (2009). *Microwave remote sensing of soil moisture – A brief introduction*. International Institute for Geo-Information Science and Earth Observation (ITC), Enschede, The Netherlands,.
- T.Schmugge, & Jackson, T. J. (1993). 2-2\_02\_Schmugge.pdf. *EARSel ADVANCES IN REMOTE SENSING*, 2(2), 5–14. Retrieved from [http://www.earsel.org/Advances/2-2-1993/2-2\\_02\\_Schmugge.pdf](http://www.earsel.org/Advances/2-2-1993/2-2_02_Schmugge.pdf)
- Tolk, A. . (2003). Permanent Wilting. In *Encyclopedia of Water Science*. Retrieved from <http://www.cprl.ars.usda.gov/pdfs/Tolk-Permanent Wilting Pt-Ency Water Sci.pdf>
- Torres, R., Snoeij, P., Geudtner, D., Bibby, D., Davidson, M., Attema, E., ... Rostan, F. (2012). GMES Sentinel-1 mission. *Remote Sensing of Environment*, 120, 9–24. doi:10.1016/j.rse.2011.05.028
- Ulaby, F. T., Moore, R. K., & Fung, A. K. (1982). *Microwave Remote Sensing Active and Passive-Volume II: Radar Remote Sensing and Surface Scattering and Emission Theory*. Retrieved from <http://infoscience.epfl.ch/record/51982>
- Ulaby, F. T., Moore, R. K., & Fung, A. K. (1986). *Microwave Remote Sensing: Active and Passive, Vol. III -- Volume Scattering and Emission Theory, Advanced Systems and Applications. Microwave Remote Sensing: Active and Passive, III*, 1100. Retrieved from <https://upcommons.upc.edu/pfc/bitstream/2099.1/6971/12/Chapter 9 - Bibliography.pdf>
- UNESCO.IHE. (2014). Mau Mara Serengeti Sustainable Water Initiative (MaMaSe). Retrieved July 29, 2014, from <http://mamase.unesco-ihe.org/partnership>
- USGS. (2006). GLCF: Shuttle Radar Topography Mission. Retrieved February 04, 2015, from <http://glcf.umd.edu/data/srtm/>
- USGS. (2008). Shuttle Radar Topography Mission. Retrieved December 04, 2014, from <http://srtm.usgs.gov/mission/missionsummary.php>
- Van der Velde, R., Salama, M. S., Pellarin, T., Ofwono, M., Ma, Y., & Su, Z. (2014). Long term soil moisture mapping over the Tibetan plateau using Special Sensor Microwave/Imager. *Hydrology and Earth System Sciences*, 18(4), 1323–1337. doi:10.5194/hess-18-1323-2014
- Van der Velde, R., Su, Z., van Oevelen, P., Wen, J., Ma, Y., & Salama, M. S. (2012). Soil moisture mapping over the central part of the Tibetan Plateau using a series of ASAR WS images. *Remote Sensing of Environment*, 120, 175–187.
- Velde, R. van der, Eweys, O. A., Nyang'acha, D. O., Gathecha, H. M., & Vekerdy, Z. (2014). *Soil moisture monitoring in the Masai Mara National Reserve and surrounding Conservancies*.
- Waithaka, J. (2004). Maasai Mara — an ecosystem under siege: an African case study on the societal dimension of rangeland conservation. Retrieved December 16, 2014, from <http://www.tandfonline.com/doi/pdf/10.2989/10220110409485838>
- Walker, J. P., Willgoose, G. R., & Kalma, J. D. (2004). In situ measurement of soil moisture: a comparison of techniques. *Journal of Hydrology*, 293(1-4), 85–99. doi:10.1016/j.jhydrol.2004.01.008
- Wood, E. F., Lin, D.-S., Troch, P. A., Mancini, M., & Jackson, T. J. (1995). Soil moisture estimation: comparisons between hydrologic model estimates and remotely sensed estimates. In B. J. Choudhury, Y. H. Kerr, E. G. Njoku, & P. Pampaloni (Eds.), *Passive Microwave Remote Sensing Of Land -Atmosphere Interactions* (pp. 77–92).

WREM International. (2008). *Mara River Basin Monograph, Mara River Basin Transboundary Integrated Water Resources Management and Development Project, Final Technical Report*. Atlanta.

## APPENDICES

### APPENDIX 2: Organic matter determination

The mass of empty porcelain cups was recorded ( $M_E$ ). A known amount of soil was measured into porcelain cups and its weight recorded ( $M_{ES}$ ), the samples were placed into oven overnight at 105°C, the weight of the dry samples was taken and the samples dried again overnight at 600°C ( $M_{EB}$ ). Equations 2 - 5 were used in calculation of the components needed to realize organic matter content. The above procedure was repeated again using different samples from KMST 2,3,4,5, and 6, this was done to improve on the confidence levels. This process used disturbed soil samples.

- Mass of dry soil

$$M = M_{ES} - M \quad (1)$$

- Mass of burned soil

$$M_A = M_{EB} - M \quad (2)$$

- Mass of organic matter

$$M_O = M - M_A \quad (3)$$

- Percentage organic matter

$$OM = \frac{M_O}{M_D} \times 100 \quad (4)$$

where;  $M_E$ =Mass of empty cup,  $M_{ES}$ =Mass of Empty + Soil,  $M_D$ =Mass of dry soil,  $M_{EB}$ =Mass of burned soil,  $M_O$ =Mass of organic matter

OM=percentage organic matter

Table 4: **Organic matter content for each KMST**

Sample Number	Cup Weight	Wet Cup+Soil	After drying 105 Celsius	Dry soil weight	After ashing 600 Celsius	Weight loss from ashing	Percentage Org. Mat.
<b>KMST_1</b>	101.73	126.72	124.31	22.58	122.43	1.88	<b>1.54</b>
<b>KMST_2</b>	104.77	128.44	126.76	21.99	125.51	1.25	<b>1.00</b>
<b>KMST_3</b>	101.9	127.56	126.42	24.52	125.53	0.89	<b>0.71</b>
<b>KMST_4</b>	105.97	131.94	130.63	24.66	129.36	1.27	<b>0.98</b>
<b>KMST_5</b>	107.75	133.51	131.48	23.73	130.07	1.41	<b>1.08</b>
<b>KMST_6</b>	106.47	134.38	131.39	24.92	129.70	1.69	<b>1.30</b>
<b>3repeat</b>	38.21	52.42	51.74	13.53	51.25	0.49	<b>0.96</b>
<b>2repeat</b>	38.21	51.37	50.46	12.25	49.77	0.69	<b>1.39</b>
<b>4repeat</b>	41.84	52.96	52.37	10.53	51.84	0.53	<b>1.02</b>
<b>6repeat</b>	40.12	52.99	51.63	11.51	50.87	0.76	<b>1.49</b>

APPENDIX 1

	<b>KMST01</b>	<b>KMST02</b>	<b>KMST03</b>	<b>KMST04</b>	<b>KMST05</b>	<b>KMST06</b>
<b>Date installed</b>	23rd September 2014	24th September 2014	24th September 2014	25th September 2014	25th September 2014	26th September 2014
<b>Coordinates</b>	Latitude: 01.32043 S Longitude: 35.03639 E Elevation: 1550 m (a.s.l.)	Latitude: 01.51988 S Longitude: 35.16982 E Elevation: 1591 m (a.s.l.)	Latitude: 01.66166 S Longitude: 35.43250 E Elevation: 1840 m (a.s.l.)	Latitude: 01.20499 S Longitude: 35.46390 E Elevation: 1908 m (a.s.l.)	Latitude: 01.45698 S Longitude: 35.38197 E Elevation: 1709 m (a.s.l.)	Latitude: 01.23306 S Longitude: 35.25944 E Elevation: 1752 m (a.s.l.)
<b>Configuration station</b>	5TM Probe Port Depth KSMST01-P01 Port 1 5 cm KSMST01-P02 Port 2 10 cm KSMST01-P03 Port 3 20 cm KSMST01-P04 Port 4 40 cm KSMST01-P05 Port 5 80 cm	5TM Probe Port Depth KSMST02-P01 Port 1 5 cm KSMST02-P02 Port 2 10 cm KSMST02-P03 Port 3 20 cm KSMST02-P04 Port 4 40 cm KSMST02-P05 Port 5 70 cm	5TM Probe Port Depth KSMST03-P01 Port 1 5 cm KSMST03-P02 Port 2 10 cm KSMST03-P03 Port 3 20 cm KSMST03-P04 Port 4 40 cm KSMST03-P05 Port 5 80 cm	5TM Probe Port Depth KSMST04-P01 Port 1 5 cm KSMST04-P02 Port 2 10 cm KSMST04-P03 Port 3 20 cm KSMST04-P04 Port 4 40 cm KSMST04-P05 Port 5 80 cm	5TM Probe Port Depth KSMST05-P01 Port 1 5 cm KSMST05-P02 Port 2 10 cm KSMST05-P03 Port 3 20 cm KSMST05-P04 Port 4 40 cm KSMST05-P05 Port 5 80 cm	5TM Probe Port Depth KSMST06-P01 Port 1 5 cm KSMST06-P02 Port 2 10 cm KSMST06-P03 Port 3 20 cm KSMST06-P04 Port 4 40 cm KSMST06-P05 Port 5 80 cm
<b>Land use and vegetation cover</b>	Installed in Masai Mara reserve. The vegetation cover is Savannah grass height was around 10 cm due to grazing by the wildlife at time of the installation which was during the dry season. The topography is very gently rolling.	Installed in the Masai Mara Reserve. The vegetation cover is Savannah grass with shrubs spread around the area. At time of the installation the grass cover had very little biomass for the same reasons as explained under KMST01. Presence of termite hills within the proximity of the station (about 100m). The topography is very gently rolling to almost flat.	KMST03 is installed in a Masai Mara Conservancy. The vegetation cover is Savannah with a dense distribution of trees and shrubs spread around the area with heights reaching more than 3 m, whereby the surface is covered with grass. The topography includes hills of some significance.	Installed in grassland outside the community owned Masai Mara Conservancy. The vegetation cover is Savannah with a sparse distribution shrubs spread around the area with heights reaching 1 up to about 2 m, whereby the surface is covered with grass. The topography consists of rolling hills.	Installed nearby the premises of the Nkolale school which is part of the Masai Mara Conservancy. The land cover is Savannah consisting of the, at time of writing, short grasses with a sparse distribution shrubs spread around the area with heights reaching 1 up to about 2 m. The topography consists of gently rolling hills.	Installed on community owned land that is part of the Masai Mara Conservancy. The vegetation cover is dominated with, at time of writing, short grasses with shrubs primarily placed to demarcate the 'property of households. The topography is flat with moderate hills at some distance (e.g. tens of kilometers).
<b>Soil profile</b>	<i>Color:</i> Color is gray and homogeneous across the 80-cm soil profile. The soil was dry at time of the installation	<i>Color:</i> Color is dark gray and homogeneous across the 70-cm soil profile. The soil was dry at time of the installation.	<i>Color:</i> The color is dark gray and homogeneous across the soil profile. Scattered brown/reddish spots were found at depths of 40 and 60 cm as an indication of iron oxidation. At 80 cm a portion of the soil is color white which indicates the presence of calcium carbonates.	<i>Color:</i> The color is dark gray and homogeneous across the soil profile. Scattered brown/reddish spots were found at depths of 40 and 60 cm as an indication of iron oxidation.	<i>Color:</i> The color is dark gray and homogeneous across the soil profile. White colored soil is found near depths of 80 cm as an indication for the existence of calcium carbonates	<i>Color:</i> The color is dark gray and homogeneous across the soil profile.

SYNTHETIC APERTURE RADAR FOR VEGETATION AND SOIL MOISTURE MONITORING IN MASAI MARA

<p><i>Texture:</i> Field observation suggested a high percentage of clay.</p> <p><i>Structure:</i> Surface layer shows a cracked soil structure with rounded clods; A block structure with large soil clods is found at depths between 30 and 70 cm;</p>	<p><i>Texture:</i> Field observation suggested a high percentage of clay. Digging of soil pits was very labor intensive.</p> <p><i>Structure:</i> The entire 70-cm soil profile is characterized by a clear block structure with large soil clods</p>	<p><i>Texture:</i> Field observation shows that the surface layer (0-10 cm) has a high percentage of clay whereas also evidence for sand and silt was found. At greater depth the percentage of finer materials (clay) increased</p> <p><i>Structure:</i> The soil is fairly loose near the surface; A block structure with small soil clods was found below depth of 20 cm.</p>	<p><i>Texture:</i> Field observation suggests that clay is found homogeneously across the soil profile.</p> <p><i>Structure:</i> The soil is fairly loose near the surface; A block structure with small soil clods was found below depth of 20 cm.</p>	<p><i>Texture:</i> Field observation suggests that clay is found homogeneously across the soil profile</p> <p><i>Structure:</i> The soil is fairly loose with rounded soil clods;</p>	<p><i>Texture:</i> Field observation suggests that clay is found homogeneously across the soil profile.</p> <p><i>Structure:</i> The soil is fairly loose with rounded soil clods;</p>
<p><i>Roots:</i> Grass root were only found in the top 5-cm. Root remnants exist at greater depths, but without visible connection to the surface. It is expected that grass roots will grow rapidly during the wet season.</p> <p><i>Gravel:</i> There is no evidence for gravel existence over the whole profile.</p>	<p><i>Roots:</i> Grass root were only found in the top 5-cm. Root remnants exist at greater depths, but without visible connection to the surface. It is expected that grass roots will grow rapidly during the wet season.</p> <p><i>Gravel:</i> about 70 % of the soil below 70 cm consisted of large rocks and for this reasons the deepest soil moisture probes was installed at 70 cm depth instead of the nominal 80 cm.</p>	<p><i>Roots:</i> Grass root were only found in the top 20-cm. Root remnants exist at greater depths, but without visible connection to the surface.</p> <p><i>Gravel:</i> Some small grained gravel was found at depth below 80 cm.</p>	<p><i>Roots:</i> Grass root were found in the top 20-cm.</p>	<p><i>Roots:</i> Grass root were found in the top 20-cm.</p>	<p><i>Roots:</i> Grass root were found in the top 20-cm.</p> <p><i>Gravel:</i> No gravel is reported.</p>